2019

In Vitro Uptake and Biodistribution of Silver Nanoparticles in Vero 76 Cells

Miriam A. Crane
Wright State University

IN VITRO UPTAKE AND BIODISTRIBUTION OF SILVER NANOPARTICLES IN *VERO 76* CELLS

A Thesis submitted in partial fulfillment of the
requirements for the degree of
Master of Science

by

MIRIAM A. CRANE

B.S., Wright State University, 2017

2019

Wright State University

WRIGHT STATE UNIVERSITY

GRADUATE SCHOOL

December 13th, 2019

I HEREBY RECOMMEND THAT THE THESIS PREPARED UNDER MY SUPERVISION BY Miriam A. Crane ENTITLED *In vitro* Uptake and Biodistribution of Silver Nanoparticles in *Vero 76* Cells BE ACCEPTED IN PARTIAL FULFILLMENT OF THE REQUIREMENTS FOR THE DEGREE OF Master of Science.

_____

Ioana E. Pavel, Ph.D.
Thesis Director

_____

David A. Grossie, Ph.D.
Chair, Department of Chemistry

Committee on Final Examination:

_____

Ioana E. Pavel, Ph.D.

_____

David A. Dolson, Ph.D.

_____

Steven R. Higgins, Ph.D.

_____

Marjorie M. Markopoulos, Ph.D.

_____

Barry Milligan, Ph.D.
Interim Dean of the Graduate School

ABSTRACT

Crane, Miriam A. M.S., Department of Chemistry, Wright State University, 2019. *In vitro* Uptake and Biodistribution of Silver Nanoparticles in *Vero 76* Cells

The number of consumer products containing nanomaterials over the last eight years has increased over two-fold. Silver is one of the most commonly used materials in consumer goods nanoparticle fabrication.[1] Thus, the uptake and biodistribution of silver nanoparticles (AgNPs) within mammalian cells can provide insight into their possible toxicological effects. In this study, starch-capped AgNPs of an average diameter of 9 ± 5 nm were synthesized via a bottom-up method, and characterized by Raman spectroscopy, transmission electron microscopy (TEM), inductively couple plasma optical emission spectroscopy (ICP-OES), and absorption spectroscopy. *Vero 76* cells were incubated with 0.0, 0.1, 1.0, and 3.0 mg L^{-1} starch-capped AgNPs for 2, 4, 12, and 24 hr in a water vehicle control for imaging with CytoViva darkfield microscopy and hyperspectral analysis. It was observed that the morphology of the cells was negatively impacted at all exposure concentrations in a dose-dependent manner. The cells appear clustered, had fewer dendrites forming, and cell debris is visible on the microscope slide. *Vero 76* cells were exposed to all concentrations of AgNPs for 4 hr at 0.0, 0.1, 1.0, and 1.5 mg L^{-1} for mitochondrial isolation and total Ag uptake was estimated by ICP-OES. It was determined that at exposure concentrations of 1.0 and 1.5 mg L^{-1}, AgNPs remained in the incubated Dulbecco's Modified Eagle Medium (DMEM), 86% and 77%, respectively. A

bicinchoninic acid (BCA) protein assay was also performed under similar conditions in order to examine cell viability. Cellular toxicity was found to be concentration dependent; the smallest cell viability value (7%) was observed at the highest concentration of AgNPs (3 mg L^{-1}).

Table of Contents

List of Figures

List of Tables

List of Schemes

Acknowledgements

I would like to acknowledge Dr. Ioana Pavel for allowing me to complete my Master of Science in her lab. I would also like to thank her for instilling the ability to independently work and critically think through my research. I want to also express my appreciation to my committee members: Dr. Higgins, Dr, Markopoulos, and Dr. Dolson, for taking the time to give advice during times of frustration and struggle. I would like to thank the WSU chemistry department for their support during my time as a graduate student. Thank you to all my colleagues within Dr. Pavel's research group; you have helped keep me motivated and semi-sane the last three years. Thank you to my family and friends that have continued to show support and love throughout my ups and downs of research. Last, but not least, I would like to thank my amazing boyfriend, Matthew Long, for the love, support, understanding and patience.

1. Introduction

1.1. Silver Nanoparticles (AgNPs)

1.1.1. Background of Silver Nanoparticles

According to the U.S. Environmental Protection Agency (EPA), a nanoparticle is characterized as a particle with at least two dimensions within the range of 1 to 100 nm.[2] The use of nanomaterials in everyday life seems unreal, yet they are found in consumer goods from health and fitness to goods for children, as well as in the medical field (Figure 1). This is largely due to nanoparticles having unique physicochemical characteristics (PCCs) when compared to the bulk material. These PCCs are: composition, size, size distribution, shape, surface area, surface chemistry, surface charge, purity, aggregation state, solubility, stability, and surface reactivity.[3] All of these characteristics can be tailored during nanofabrication by means of the choice of reducing agent and capping agent. According to the Consumer Product Inventory issued by The Project on Emerging Nanotechnologies, the nanotechnology sector has vastly grown to over a trillion dollars.[4,5] With the growth of this industry, the possible impact of nanoparticles on humans and the environment became an important topic of research and discussion around the world.

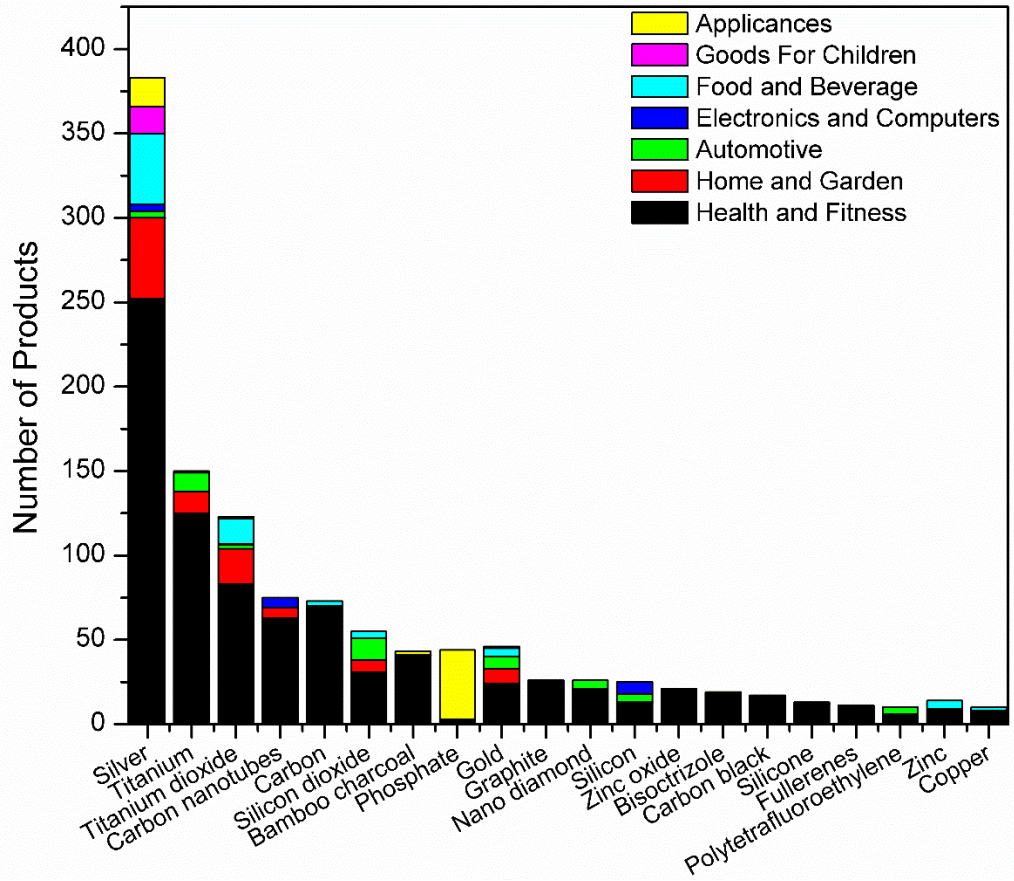

Figure 1. Total number of consumer goods containing nanomaterials by material (N = 383, N = 150, N = 123, N = 75, N = 73, N = 55, N = 43, N = 44, N = 46, N = 26, N = 26, N = 25, N = 21, N = 19, N = 17, N = 13, N = 11, N = 10, N = 14, and N = 10, respectively) and category. (Charts reconstructed by Miriam Crane from data in The Nanodatabase)[1]

The most commonly used metal in the nanoparticle fabrication is silver. This is due to its antimicrobial and antibacterial properties (Figure 1).[6,7] Studies on Gram-positive and Gram-negative bacteria show that AgNPs have inhibitory and bactericidal effects.[8,9] Numerous *in vivo* and *in vitro* studies have found that AgNPs have cytotoxic and genotoxic effects in both animal and human cell lines.[10,11,12,13,14] While there is no EPA standard limiting the amount of AgNPs within consumer goods, there is a limit set for ionic silver in drinking water of 0.10 mg L^{-1} (i.e., the Secondary Maximum Contaminant

Level).[15] Thus, the mechanism by which the AgNPs are causing cellular toxicity is of great interest.

1.1.2. Common Fabrication Techniques of Nanoparticles

There are numerous fabrication methods for AgNPs, but two main techniques are top-down and bottom-up approaches (Figure 2).

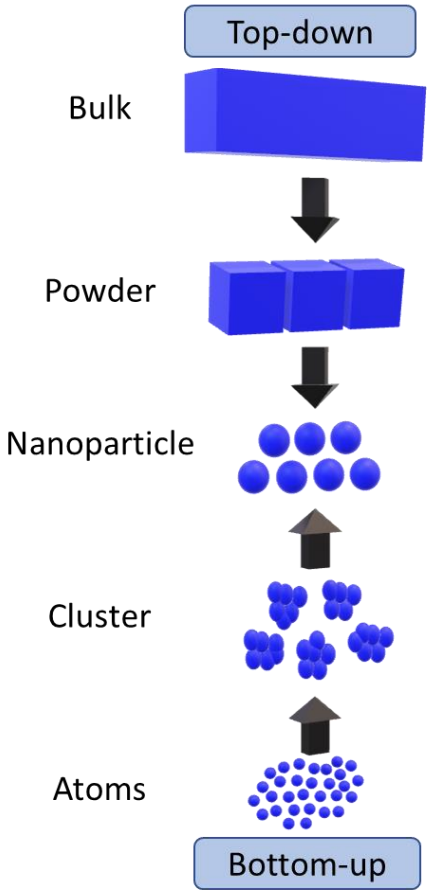

Figure 2. Top-down and bottom-up approaches for nanoparticle fabrication.

The top-down technique is the process of taking a bulk material and breaking it down by means of finer and finer tools to a smaller scale until the nanoscale level is reached. This can be done by means of mechanicanosynthetic methods, thermal methods, and chemical fabrication. Mechanicanosynthetic methods include ball milling by abrasion, compaction

and consolidation, which are used to make nanocomposites. The mechanical top-down methods are largely employed in industry because they are less expensive to scale-up to production volumes. The thermal methods such as laser ablation, arc discharge, solar flux, and plasma methods require an excessive high energy input; therefore, the potential for scale-up and quality control are restricted. Top-down chemical fabrication methods are widely utilized in industry because of the scale-up is easier to implement. Other chemical fabrication methods commonly exploited in industry include anodizing, lithography, and nanoimprint lithography.

The bottom-up technique starts at the atomic or molecular level and is driven by a natural physical property or an applied external force to give rise to larger, more organized systems. Chemical vapor deposition, atomic layer deposition, and molecular beam epitaxy are used in industry. Electrodeposition and electroless deposition are simple ways to manufacture various forms of nanomaterials. Numerous liquid phase methods are low cost and can be scaled-up.[16] Thus, the liquid phase method is selected for the fabrication of AgNPs in this thesis.

1.1.3. Background on Starch-Capped AgNPs

As mentioned above, a liquid phase method was selected to fabricate starch-capped AgNPs. The cytotoxicity and genotoxicity of these AgNPs have been studied in zebrafish, human cells, and bacteria models, just to name a few.[10, 17] This is a green method for nanomaterials fabrication as it uses nontoxic reducing/capping agent(s), environmentally benign solvents, and/or renewable materials. The reducing/capping agent in this thesis work is a soluble polysaccharide, namely potato starch (Figure 3). This reducing/capping agent is nontoxic, environmentally friendly, and widely available.

In a previous study, starch alone (2.8% w/v) was found to have no cytotoxic effect in normal human lung fibroblasts and human glioblastoma cells, thus confirming its biocompatibility.[11] Amylose is a soluble starch, which in aqueous solutions forms a left-handed helical conformation chain with linkages α (1→4) between D-glucose subunits.[17,18]

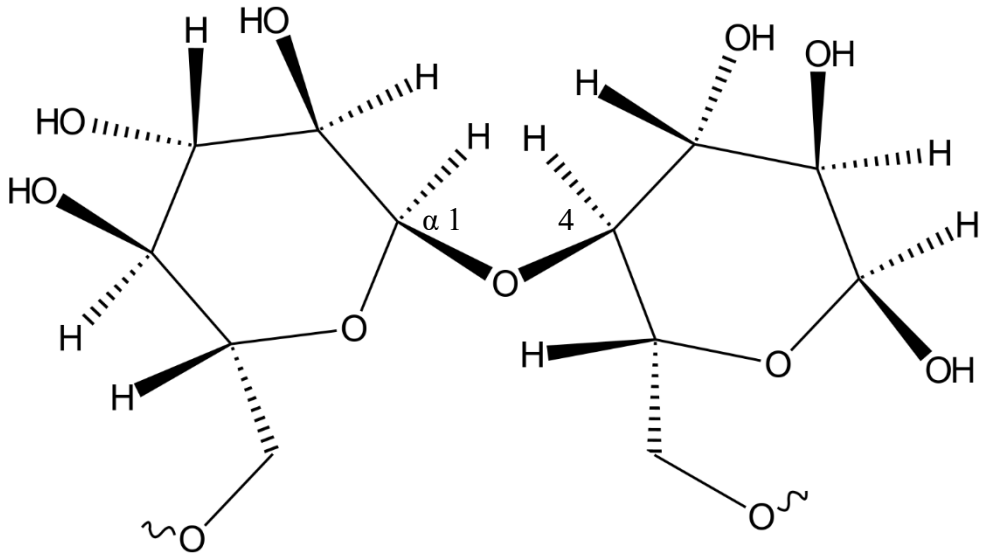

Figure 3. Depiction of the structure of amylose chain formed by the α (1-4) linkages between D-glucose subunits (Structure made via ChemDoodle).

Due to its conformation in water, starch behaves as a linear polymer by forming films and complexes with ligands. The theorized mechanism of reduction of silver nitrate is by its reaction to the terminal aldehyde of the starch and stabilization of the nanoparticle by the starch itself.[19]

1.2. Mammalian Cell Biology Background

Mammalian cells are eukaryotic cells; this means that the cell contains organelles that carry out specialized functions. Each organelle is bound by a membrane, which controls the flow of molecules and ions into/out of the cell and thereby maintains its specialized

environment. The structure of a mammalian cell and the various types of organelles are displayed in Figure 4.

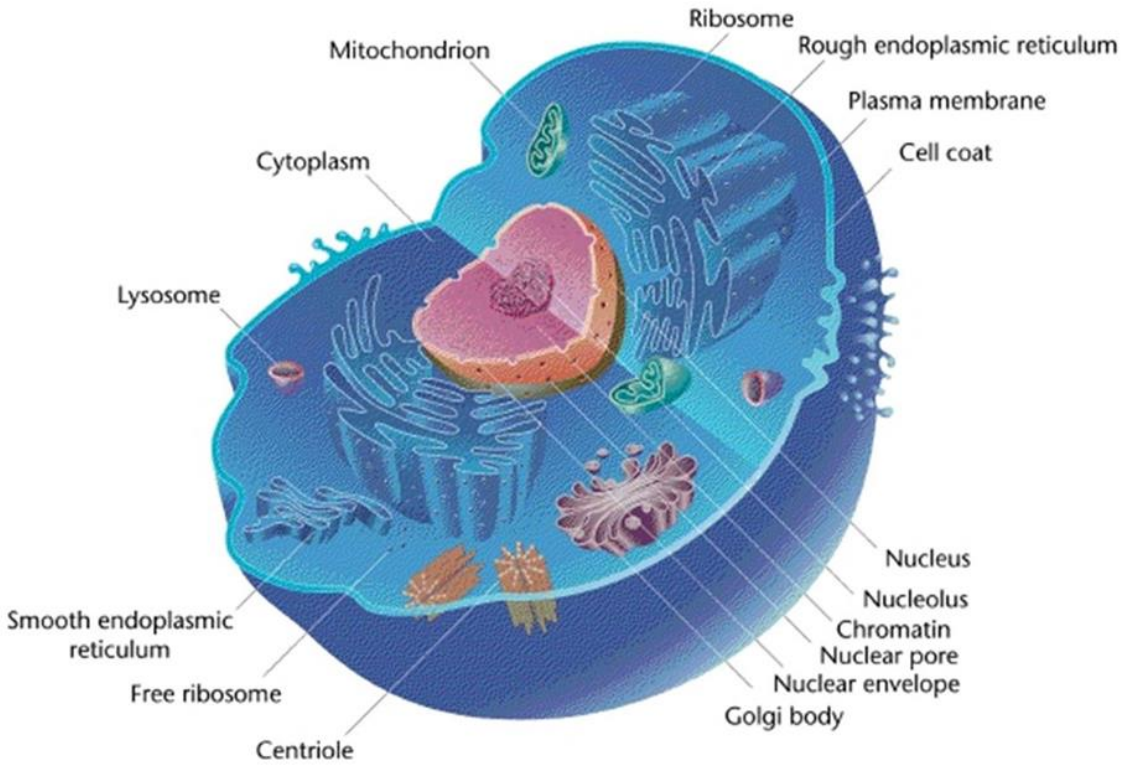

Figure 4. Depiction of a mammalian cell with its various organelle labeled (purchased by Miriam Crane on stockphotos.com; Order # 73684).

Briefly, the main organelles of mammalian cells are the endoplasmic reticulum (ER), Golgi body, ribosomes, nucleus, centriole, mitochondrion, plasma membrane, and cytoskeleton. The ER, Golgi body and ribosomes are composed of polypeptide chains and lipids. The cytoskeleton contributes to cell shape and movement, where the plasma membrane selectively controls what moves in and out of the cell. The centrioles are associated with cell division. The nucleus houses, protects, and controls access to the deoxyribonucleic acid (DNA). Mitochondria are responsible for key stages of cellular respiration, including the citric acid cycle and oxidative phosphorylation. It is the main

site for adenosine triphosphate (ATP) production, which provides the energy source for the cell. Understanding the interactions between AgNPs and mitochondria will give insight into key toxic effects.

Mammalian cells undergo a process called endocytosis to ingest nutrients, fluids, and other molecules needed for survival (Figure 5).[20]

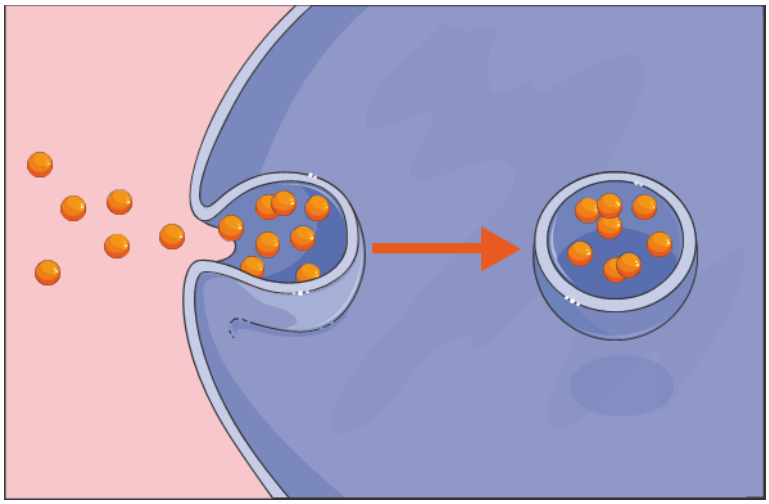

Figure 5. Macromolecules being internalized by the process of endocytosis. (Figure courtesy of SERVIER Medical Art, https://smart.servier.com/)

Macromolecules are internalized by the plasma membrane surrounding the nutrients, which buds off inside the cell forming what is called a vesicle. Once the macromolecule is inside the cell, catabolism, i.e., the degradation of complex molecules into simpler ones by means of enzymatic breakdown, takes place in lysosomes. Digestion of the macromolecule into its subunits allows for the cell to utilize them for glycolysis (derived from the Greek words *glykys*, "sweet", and *lysis*, "splitting"), which takes place in the cytosol. The next two stages of cellular respiration, the citric acid cycle and oxidative breakdown, happen solely in the mitochondria.[21]

1.2.1. Structure and Function of Mitochondria

As mentioned previously, mitochondria of a cell are the main site for energy production in the form of ATP, which is produced through cellular respiration. Figure 6 displays the structural components of a mitochondrion.

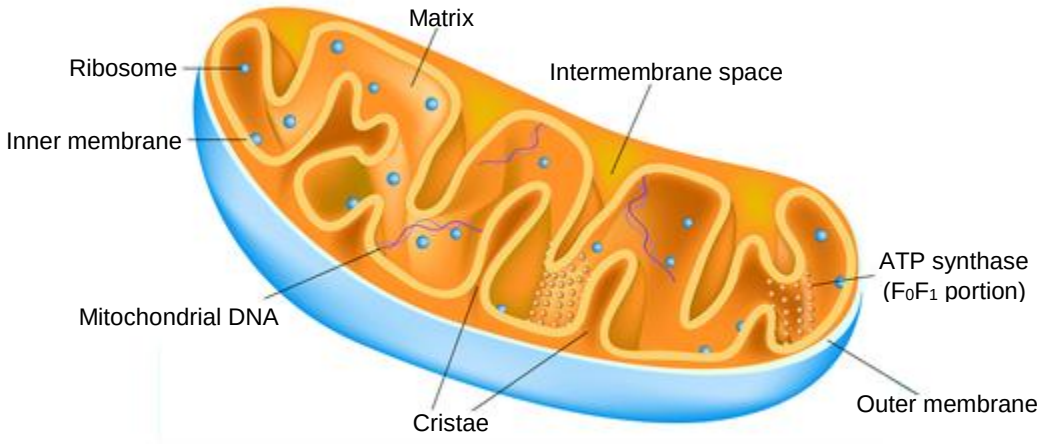

Figure 6. Representation of a mitochondrion and its specific parts (purchased by Miriam Crane on stockphoto.com; Order 106975).

The mitochondrion has four separate compartments within its structure: outer membrane, inner membrane, matrix, and intermembrane space. A unique set of proteins can be found in each compartment that enable it to perform its function. Both the outer and inner membrane are composed of phospholipid bilayers with their unique set of proteins imbedded into them. The outer membrane contains channel-forming proteins called porin, which form wide aqueous channels through the lipid bilayer and make the membrane permeable to molecules less than 5,000 Daltons. The inner membrane is highly folded into cristae, which contain proteins to carry out oxidation reactions during the electron-transport chain on the membrane and ATP synthase that produces ATP

molecules within the matrix of the mitochondrion. The inner and outer membranes form an intermembrane space between the two of them; this contains several enzymes that use the ATP passing out of the matrix to phosphorylate other nucleotides. The matrix is comprised of a highly concentrated mixture of enzymes required for oxidative reactions as well as other metabolic pathways. All these compartments play a key role in the citric acid cycle and the electron transport chain (i.e., oxidative phosphorylation). Figure 7 depicts two key parts of cellular respiration: the electron transport chain and the citric acid cycle.[21]

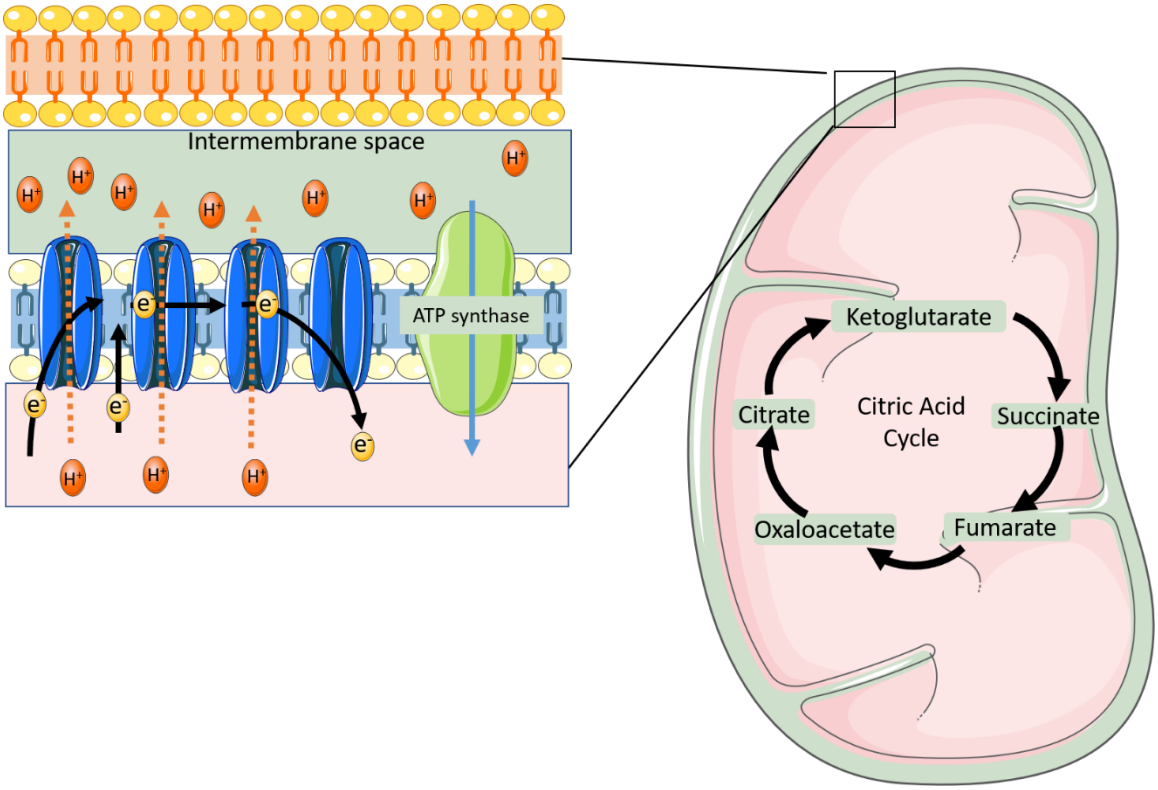

Figure 7. Depiction of the citric acid cycle and the membrane-based mechanism of the electron-transport chain of mitochondria. (Figure constructed with images courtesy of SERVIER Medical Art, https://smart.servier.com/)

The first part of cellular respiration, glycolysis, takes place in the cytosol of the cell and breaks down simple subunits to pyruvate. Pyruvate is pumped into the mitochondrial matrix, where it undergoes decarboxylation by three enzyme complexes (the pyruvate dehydrogenase complex) to produce reduced nicotinamide adenine dinucleotide phosphate (NADH), carbon dioxide (CO_2), and acetyl Coenzyme A (CoA). Acetyl CoA then enters the citric acid cycle where it undergoes oxidative breakdown to form NADH and flavin adenine dinucleotide ($FADH_2$). Both NAD^+ and FAD are important high-energy electron carriers, in their reduced form they carrier electrons and hydrogen. NADH and $FADH_2$ transfer the electrons to the last step in the oxidation of nutrients: the electron transport chain. This is the step in which most chemical energy of a cell is produced in the form of ATP. The electron transport chain is a membrane-based mechanism, meaning the complexes are embedded within the phospholipid bilayer of the inner membrane of the mitochondrion. Ions are transported across the membrane by four protein complexes; the electron transfers release energy used to pump protons (H^+) from omnipresent water within the cell across the membrane generating an electrochemical proton gradient. The H^+ flow back into the matrix through a protein complex called ATP synthase, which catalyzes the energy required for the synthesis of ATP from adenosine diphosphate (ADP) and inorganic phosphate. If the metabolic reactions and processes are interrupted, this can cause the cells' ATP content to drop, meaning possible apoptosis (cell death) could occur.[21]

1.3. Background on *Vero 76* Cell Line

The biological matrix chosen for this project was *Vero 76* cells, which were derived from a kidney of a normal adult African Green monkey (*Cercopithecus aethiops*) in the 1960s.

This cell line is well established in continuous mammalian cell research. The characteristics of this cell line are that they are anchorage-dependent, dendritic, and must be cultured before 100 % confluency (amount of cell culture dish covered by cells) is reached or cell death will occur.[22] Figure 7 displays an image of the cells at approximately 70 % confluency, note the dendric shape. These dendrites allow for the cells to communicate.

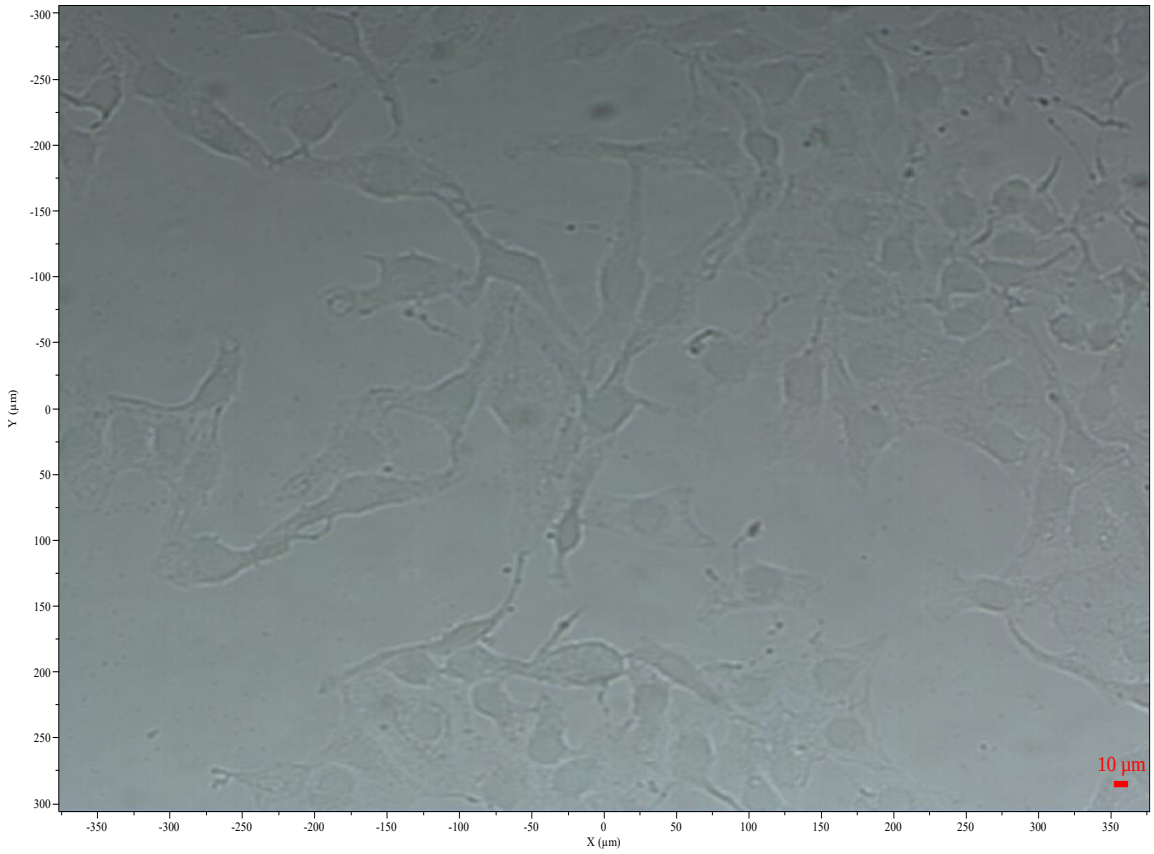

Figure 8. Optical image of a monolayer of Vero 76 cells grown to ~ 70 % confluency.

1.4. Knowledge Gaps

The biomedical applications of AgNPs are limited by the lack of well-established methodologies for studying their cellular translocation and possible transformations.

1.5. Main Goal and Specific Aims

Main Goal:

Quantify total silver absorbed by whole *Vero 76* cells and their mitochondria via ICP-OES and follow silver nanoparticle distribution by hyperspectral CytoViva imaging. It is thought that as concentration exposure of AgNPs and time of incubation are increased, the cytotoxic effects will increase.[10,17]

Specific Aim 1:

Synthesize, purify, and characterize starch-capped AgNPs via centrifugation and tangential flow filtration (TFF), ultraviolet and visible absorption spectroscopy (UV-Vis), transmission electron microscopy (TEM), CytoViva hyperspectral microscopy, Raman spectroscopy, and inductively coupled plasma-optical emission spectroscopy (ICP-OES).

Specific Aim 2:

Isolate and determine total cellular protein content of whole *Vero 76* cells and their mitochondria before and after exposure to colloidal AgNPs via a mitochondrial isolation assay.

Specific Aim 3:

Quantify the total silver content within these biological matrices by ICP-OES and monitor nanoparticle distribution by hyperspectral CytoViva imaging.

2. Method

2.1. Chemicals and Materials

Silver nitrate (> 99%, solid, $AgNO_3$) was manufactured by Acros Organics. A trace metal grade ICP-OES silver standard (1.00×10^3 mg L^{-1}) was purchased from CentraPrep. Trace metal grade nitric acid (70%, TM HNO_3) and soluble starch (powder, $C_{12}H_{22}O_{11}$) were acquired from Fisher Scientific. All chemicals and reagents were used as received, without any further purification. High quality water (> 18 MΩ cm, HQ H_2O) was utilized as a solvent.

Vero 76 cells (ATCC® CRL #1587™) were procured from American Type Culture Collection. Dulbecco's Modified Eagle's Medium/High Glucose (DMEM), penicillin-streptomycin glutamine (100x, PS), and trypsin (0.05%) with EDTA (0.53 M) were obtained from HyClone. Fetal bovine serum (FBS) was purchased from Corning. Phosphate buffered saline (1x, PBS), hydrogen peroxide (30%), and formaldehyde (37%) were acquired from Fisher Bioreagents. MitoTracker red CMXRos (MT red) was attained from Invitrogen. Mitochondrial isolation kit and bicinchoninic acid (BCA) protein assay were manufactured by Thermofisher.

2.2. AgNP Synthesis and Purification

2.2.1. Synthesis and Purification via Centrifugation

Starch-capped AgNPs were synthesized by a one-pot green synthesis method in an autoclave bottle.[19] Briefly, 1.0 g of soluble starch was dissolved through heating in 100 mL of HQ H_2O on a hot plate at ~ 90° C for ~ 1 hr. Afterward, 1 mL of $AgNO_3$ solution (100 mM) was added all at once and mixed through manual stirring. The resulting mixture was immediately autoclaved at 15 psi and 121 °C for 20 min. The resulting colloid was light-yellow in color (Figure 9A), which confirmed the formation of AgNPs. After cooling to room temperature, the colloid was passed through a 0.2 μm syringe filter (Figure 9B). The colloid was then centrifuged at 14,000 rpm (22,789 g) for 1 hr and the resulting pellet containing AgNPs was washed twice with HQ H_2O through similar centrifugation in order to remove excess starch (Figure 9C-9E). AgNPs collected at each step of the centrifugation process in the pellet were redispersed through ultrasonication (output power of 25-43 Watts) for ~ 20 to 30 s into fresh HQ H_2O. The purified colloid maintained its characteristic light-yellow color (Figure 9F) and was filtered after a 24 hr stabilization period.

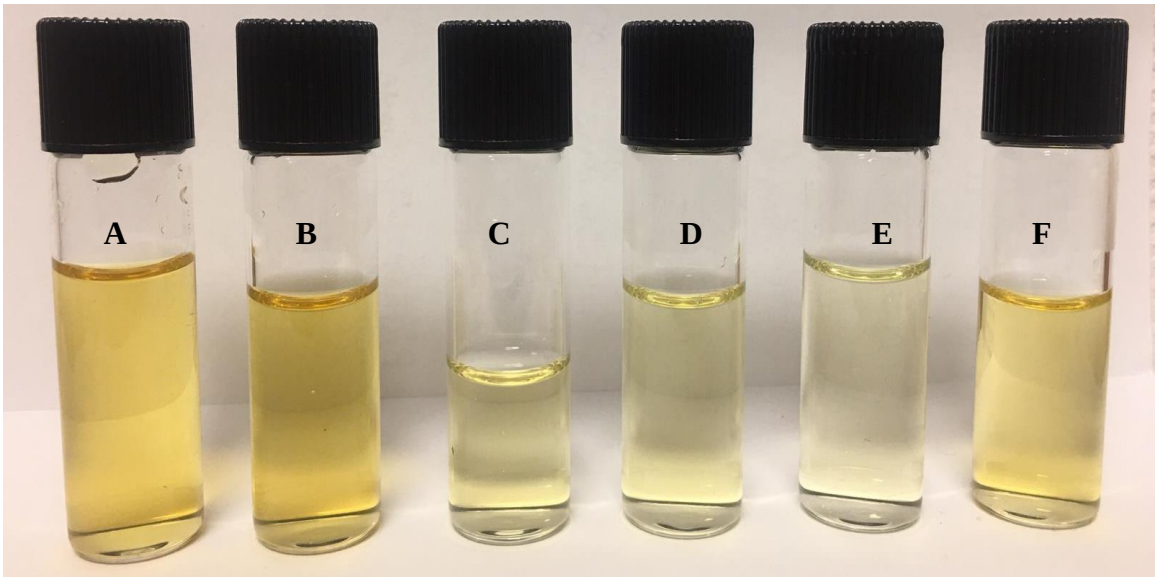

Figure 9. Image of original colloid (A), 0.2 μm permeate (B), supernatant (C), wash #1 supernatant (D), wash #2 supernatant (E), and redispersed pellet for TFF process (F).

2.2.2. Size-Selection, further Purification, and Concentration via Tangential Flow Filtration (TFF)

The TFF process was applied as described in literature.[23] In this study, the size selection, further purification, and concentration of the centrifuged AgNPs colloid (80 mL) was achieved manually through a one-step tangential filtration (Scheme 2.1) with a 70 kD modified polyetherethersulfone Midi Kros filter module (115 cm^2, > 10 nm pore size, from Spectrum Labs, Inc.) and polypropylene syringes for sample injection (Figure 10A). The final 70 kD retentate of starch-capped AgNPs maintained its characteristic color (Figure 10B) and was used in cell experiments within one week from filtration.

Scheme 2.2-1. Flow diagram for tangential flow filtration of AgNPs.

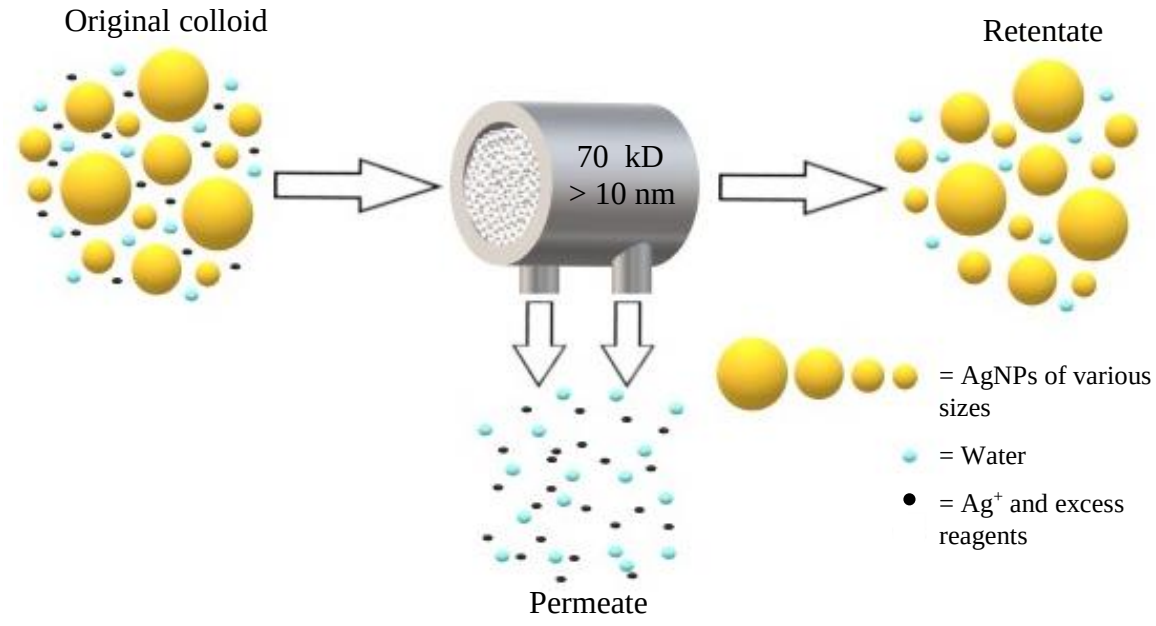

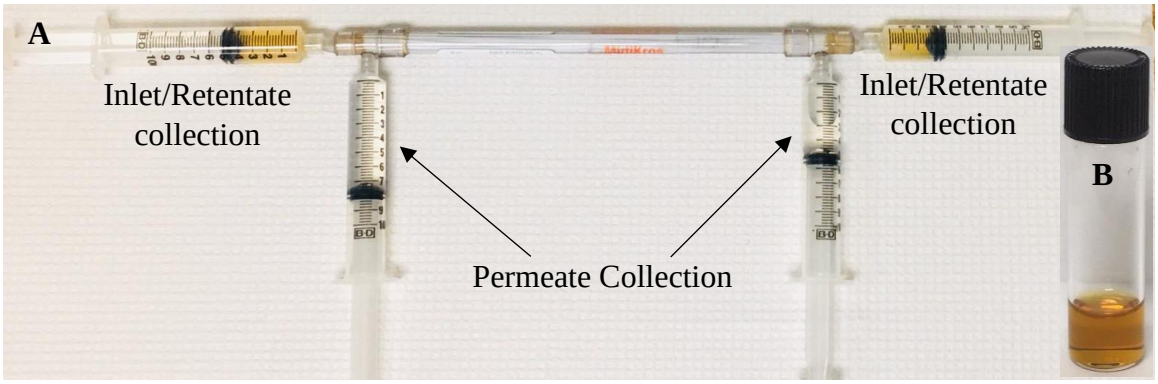

Figure 10. Image of the TFF setup (A) and the final 70 kD retentate of AgNPs for cellular experiments (B).

2.3. AgNPs Characterization

Ultraviolet and visible (UV-Vis) absorption spectroscopy, inductively coupled plasma optical emission spectroscopy (ICP-OES), Raman spectroscopy, Transmission Electron Microscopy (TEM), and CytoViva Hyperspectral microscopy were employed for the characterization of the concentrated AgNP colloid.

2.3.1. Ultraviolet and Visible (UV-Vis) Absorption Spectroscopy

A Varian Cary 50 Bio UV-Vis spectrophotometer was utilized to collect the absorption spectra of colloidal samples (200-800 nm) in disposable cuvettes (1 cm optical path), at a fast scan rate (spectral resolution of 1 nm). Absorption readings in the UV-range, a quartz cuvette (1 cm optical path) was utilized. All spectra were baseline corrected with respect to water before analysis in Origin 8 software.

2.3.2. Inductively Coupled Plasma Optical Emission Spectroscopy (ICP-OES)

In preparation for ICP-OES measurements, an acid digestion was performed on all colloidal samples of interest. A 10 µL sample aliquot was added to 5 mL of TM HNO_3 at room temperature and allowed to cold digest for 10 min. The sample was then heated on a hot plate at ~ 275° C to evaporate the acid solvent, until approximately 10 µL of sample remained. Once cooled to room temperature, the sample was quantitatively rinsed into a 10 mL volumetric flask with 286 µL of TM HNO_3 to a final 2% HNO_3 matrix. An external calibration was performed using 10 standards ranging from 0 – 350 µg L^{-1}, which were made from an ionic silver standard (1,000 mg L^{-1}) by quantitative dilutions in 2% HNO_3 acid matrix.

ICP-OES analysis was performed on a Varian 710-ES system under the following operating conditions: wavelengths of 328.068 nm and 338.289 nm for silver emission, plasma flow of 15.0 min^{-1}, auxiliary flow of 1.50 L min^{-1}, and radio frequency power of 1.2 kW. Samples were measured in triplicate with a replicate acquisition time of 15 s, an internal stabilization time of 40 s, and an uptake delay time of 45 s.

2.3.3. Raman Spectroscopy

Colloidal samples were placed into a 2 mL quartz cuvette (1 cm optical path) to collect their Raman spectra on a Horiba LabRam HR800 Raman spectrometer with an excitation line of 532 nm from a Nd: YAG green internal laser (15 mW output). Data was collected from 100-4000 cm^{-1}, utilizing the confocal Raman BX41 microscope, Olympus 100x and 50x objectives, a confocal hole of 300 μm, a holographic grating of 600 grooves mm^{-1}, and a thermoelectrically cooled Andor CCD camera (1024 x 256 pixels). The acquisition times and number of cycles were 3 s and 3, respectively. The spectral resolution in each measurement was ~ 1 cm^{-1}. Data was collected on LabSpec v.5 software and analyzed using Origin 8 software.

2.3.4. Transmission Electron Microscopy (TEM)

A 5 μL colloidal sample was drop casted onto a 300-mesh copper grid equipped with a lacey carbon support film and allowed to sit at room temperature for 24 hr in a desiccator for subsequent drying. AgNP samples were analyzed on a Philips EM 208S TEM coupled to a high resolution Gatan Bioscan camera; all images were captured under a 70-kV electron beam. ImageJ and Origin 8 software were employed for particle analysis and size distribution plots, respectively.

2.3.5. CytoViva Hyperspectral Imaging

A 5 μL sample was placed onto a glass microscope slide, covered with a microscope coverslip, and allowed to air dry for 15 to 20 min, then sealed with clear nail polish. Images were collected with 10x air, 60x and 100x oil immersion objectives on an Olympus BX 53 CytoViva enhanced dark field microscope and the Ocular software. The ENVI software was employed for the hyperspectral data collection with exposure time

varying from 0.5–1.0 seconds and 696 x 696 pixels. Data was analyzed using Origin 8 software.

2.4. Preparation and Analysis of *Vero 76* Cells

2.4.1. Culture cells

Adherent *Vero 76* cells were grown in 100 mm petri dishes, in complete growth media made up of 89% DMEM, 10% FBS, and 1% PS. The cells were incubated at 37° C in a 5% CO_2 environment and were cultured to ~ 75% confluency before splitting or counting.

2.4.2. Total Cellular Protein Determination

Colorimetric detection and quantitation of total protein within a sample for the purpose of determining percent of viable cells was performed via a bicinchoninic acid (BCA) assay kit. A set of 9 external calibration standards ranging from 0 – 2,000 mg L^{-1} were prepared from a bovine serum albumin stock of 2 g L^{-1} by quantitative dilutions in 1x PBS. Cells were harvested by trypsinization with 10 mL of trypsin for 4 min and subsequent centrifugation at ~1,243 rpm (630 g) for 10 min. The supernatant was removed, and the cell pellet was redispersed into 2 mL of 1x PBS. This was followed by the addition of 2 mL of NaOH solution (1 mM) for lysing purposes. The standards and cell samples of interest (25 µL of each) were then placed in a 96-well plate and 200 µL of a proprietary reagent mix (50:1 ratio of Reagent A to Reagent B) was added to each well. After incubation at 37 °C for 30 min in the cell incubator, the light absorbance was measured at 562.0 nm via a Varian Cary 50 microplate reader extension of the Varian Cary 50 Bio UV-Vis spectrophotometer. Total cellular protein content was determined before and after exposure to AgNPs.

2.4.3. Staining with MT-red, Exposure to AgNPs, and Fixing Cells for CytoViva Hyperspectral Microscopy

Vero 76 cells were grown on glass coverslips in 35 mm petri dishes for 12-24 hr prior to staining with MT-red. Two milliliters of 150 nM MT-red dye were added and incubated at 37° C in a 5% CO_2 environment for 30 min. Residual dye was removed by washing three times with 1x PBS solution. Cells were then exposed to varying final well concentrations (0, 0.1, 1, and 3 mg L^{-1}) of AgNPs and incubated at 37° C in a 5% CO_2 environment for 2, 4, 12, and 24 hr. After exposure to AgNPs, the cells were washed three times with DMEM, followed by three washes of 1x PBS to remove any residual AgNPs. Cells were then fixed in a 3.7% formaldehyde solution that was pipetted directly onto the coverslip and allowed to sit for 20 min in the dark. The cells were then washed three times with 1x PBS to remove any residual formaldehyde. A drop of 1x PBS was pipetted onto a clean glass microscope slide, the coverslip was placed onto the slide, and sealed with clear nail polish. The analysis parameters were the same as stated above (Section 2.3.4). Fluorescence emission analysis was also performed using a triple pass filter and a Prior Lumen 200 light source. Data was processed using GIMP and Origin 8 software.

2.4.4. Preparation of ICP-OES samples

Vero 76 cells were grown in tissue culture flasks (surface area175 cm^2) until ~ 75% confluent. Cells were then exposed to various concentrations (0, 0.1, 1, and 1.5 mg L^{-1}) of AgNPs and incubated at 37° C in a 5% CO_2 environment for 4 hr before harvest. The AgNP containing media was first removed by pipet and a sample aliquot was saved for

further analysis. The plate was then washed with PBS (1x) to remove any residual AgNPs; all washings were saved for analysis.

Approximately 10 mL of trypsin was added to the T-flask and incubated for 4 min at 37° C in a 5% CO_2 environment. Trypsin cleaves the proteins that are responsible for adhering the *Vero 76* cell to the plate. After 4 min, the plate was removed from the incubator and 40 mL of fresh media was added to the plate to inhibit the trypsin. The cell suspension was pipetted up and washed down the flask three times, then pipetted up and down a total of six times, with a final washed down to ensure the cell suspension was thoroughly mixed. The cell suspension was centrifuged at ~1,243 rpm (630 g) for 10 min to obtain a cell pellet. The supernatant was pipetted off and saved for ICP-OES analysis. The pellet was then used for mitochondrial isolation.

Mitochondrial isolation was performed by means of a mitochondrial isolation kit for cultured cells. The pellet was redispersed in 2 mL of DMEM and transferred to a 2 mL micro-centrifuge tube. The cell suspension was centrifuged at 3,057 rpm (900 g) for 2 min to repellet the cells. The supernatant was then removed, and reagent A (800 µL) was added. The pellet was vortexed at 1,500 rpm (6 g) for 5 seconds and incubated on ice for 2 min. Reagent B (10 µL) was added, and vortexed at 3,000 rpm (25 g) for 5 seconds. The cell suspension was incubated on ice for 5 min while vortexed at 3,000 rpm (25 g) every minute. Reagent C (800 µL) was added to the cell suspension, the tube was inverted several times followed by centrifugation at 2,696 rpm (700 g) for 10 min. The supernatant was then transferred to a new 2 mL micro-centrifuge tube and centrifuged at 3,530 rpm (12,000 g) for 15 min. The resulting supernatant was removed by pipetting. Reagent C (500 µL) was then added to the pellet and centrifuged at 3,530 rpm (12,000 g)

for 5 min. The supernatant was removed leaving the isolated mitochondria pellet. The isolated mitochondria were redispersed in 2 mL of 1x PBS, and vortexed until homogeneous. Aliquots were collected at each step in the mitochondrial isolation for ICP-OES analysis. The ICP-OES samples were prepared via the method described above, apart from 2 mL of 30% hydrogen peroxide for bleaching purposes prior to evaporating the sample with heat. The analysis parameters were the same as stated above (Section 2.3.2).

3. Results and Discussion

3.1. Characterization of AgNPs

In order to confirm the presence of AgNPs in the original colloid, UV-Vis absorption spectroscopy was performed on all supernatants associated with the centrifugation process and the TFF products. Absorption spectra of the original colloid, 0.2 µm filtrate, supernatant/washes of pellet and the final 70 kD retentate AgNPs are shown in Figure 11.

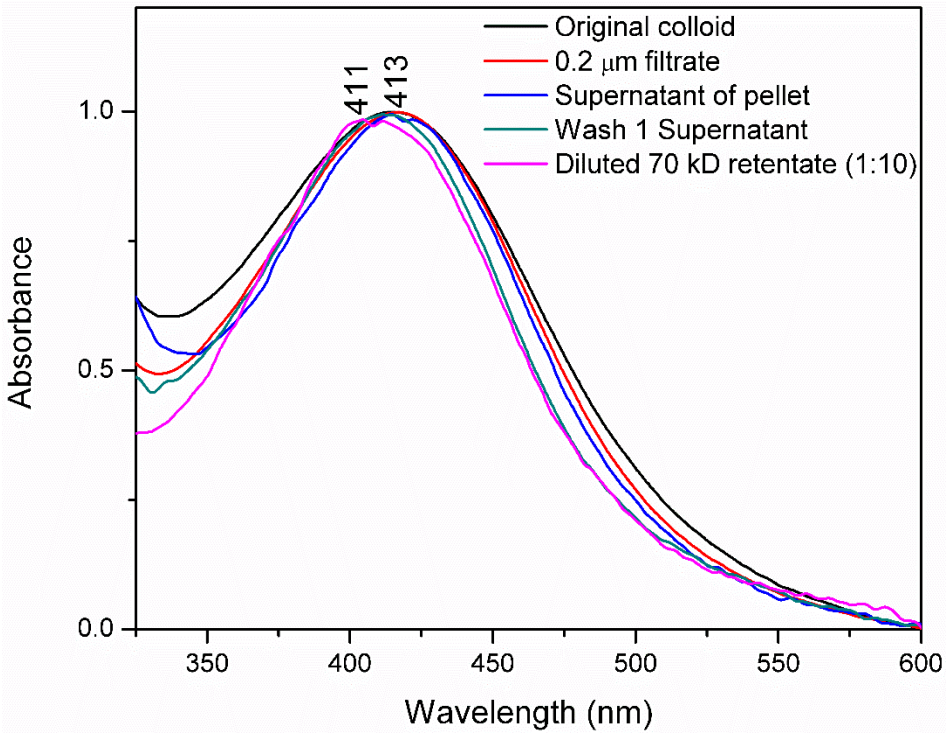

Figure 11. UV-Vis absorption spectra of original colloid, 0.2 µm permeate, supernatant/wash of pellet and diluted 70 kD retentate (1:10) showing the characteristic Surface Plasmon Resonance peak (SPR) peak of AgNPs.

The present of the Surface Plasmon Resonance (SPR) peak at 413 nm confirms the formation of colloidal AgNPs. The SPR peak suggests the AgNPs are spherical in shape.

The characteristic SPR peak was maintained throughout the centrifugation and TFF manipulation processes. A small shift in the SPR peak (411 nm) was seen after the TFF process was applied. This is probably an indication of the reduction in the average size of AgNPs after filtration as a result of the removal of larger AgNPs or AgNPs-aggregates.

To confirm excess starch was removed during the centrifugation process, UV-Vis was performed on all supernatants associated with the centrifugation process, the 70 kD retentate TFF product, and a 1% starch solution for comparison (Figure 12).

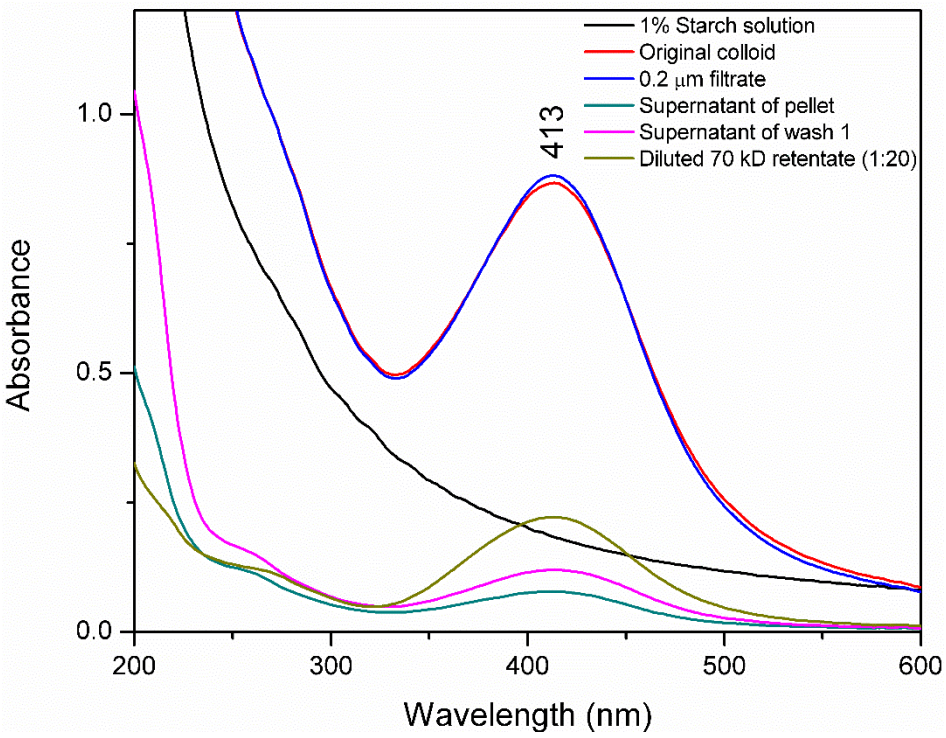

Figure 12. UV-Vis absorption spectra of 1% starch solution, original colloid, 0.2 μm filtrate, supernatant/washes, and diluted 70 kD retentate (1:20) starch-capped AgNPs showing the removal of starch throughout the centrifugation and TFF processes.

The 1 % starch solution had an absorbance greater than 1, but it is seen that starch absorbs in the UV range. The spectrum corresponding to the original starch-capped AgNPs, after the SPR peak, has an absorption in the UV range characteristic to starch.

After the centrifugation process, the profile of the UV-vis spectrum of the 70 kD retentate starch-capped AgNPs profile changes in the UV region, and the SPR remains the same, this is indicative of excess starch being removed from the colloid. The supernatant of wash 1 absorbs in the UV range, consistent with the characteristic spectra of starch, confirming excess starch was removed.

To confirm that the filtered colloid was pure and free of excess reagents, Raman spectroscopy was performed on the 70 kD retentate. The Raman spectrum of the final 70 kD retentate of starch-capped AgNP colloid is shown in Figure 13.

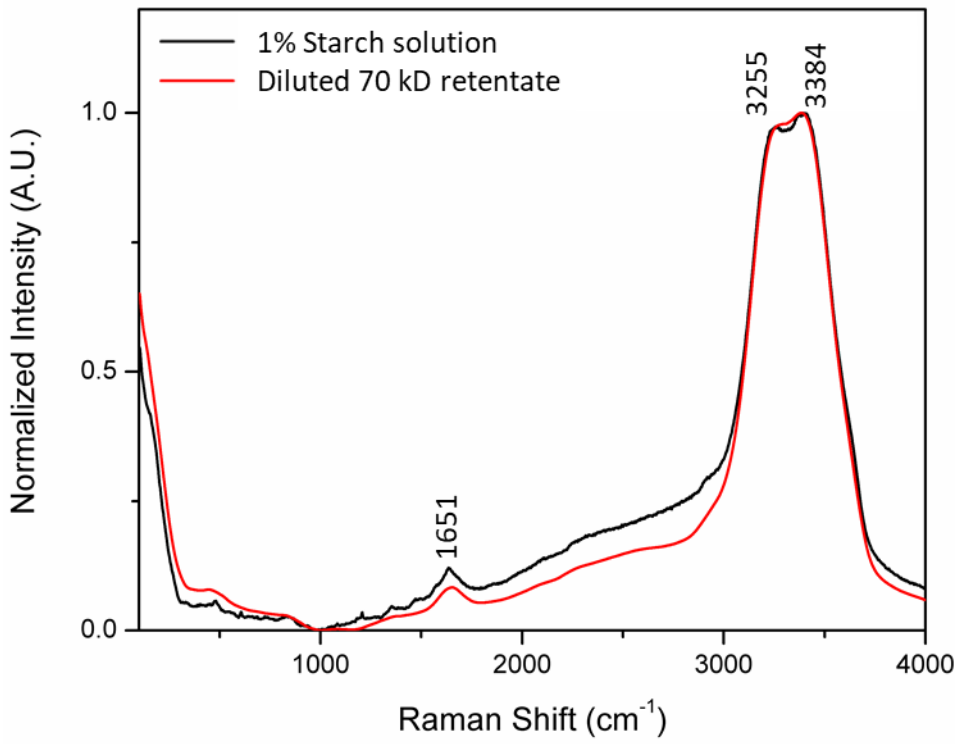

Figure 13. Raman spectrum of 1% starch solution and diluted 70 kD retentate starch-capped AgNP colloid showing characteristic peaks corresponding to water, thus confirming purity.

The observation of peaks characteristic to water confirmed the purity of colloid. The smallest peak at ~1651 cm^{-1} corresponds to the - OH bending mode, the shoulder at

~3255 cm^{-1} is due to the symmetric - OH stretch, and the most intense feature at ~3384 cm^{-1} results from the asymmetric - OH stretch.[24] The Raman spectrum for the 1% starch solution utilized for the reduction and capping of the AgNPs is shown for comparison. It should be noted that two peaks below 1000 cm^{-1} are in both spectra, this might be due to the starch.

In order to determine the concentration of the AgNPs colloid, ICP-OES measurements were performed on the original colloid and the aliquot samples collected at every step of the centrifugation and TFF processes. The 10-point external calibration curve used for ICP-OES analysis is displayed in Figure 14.

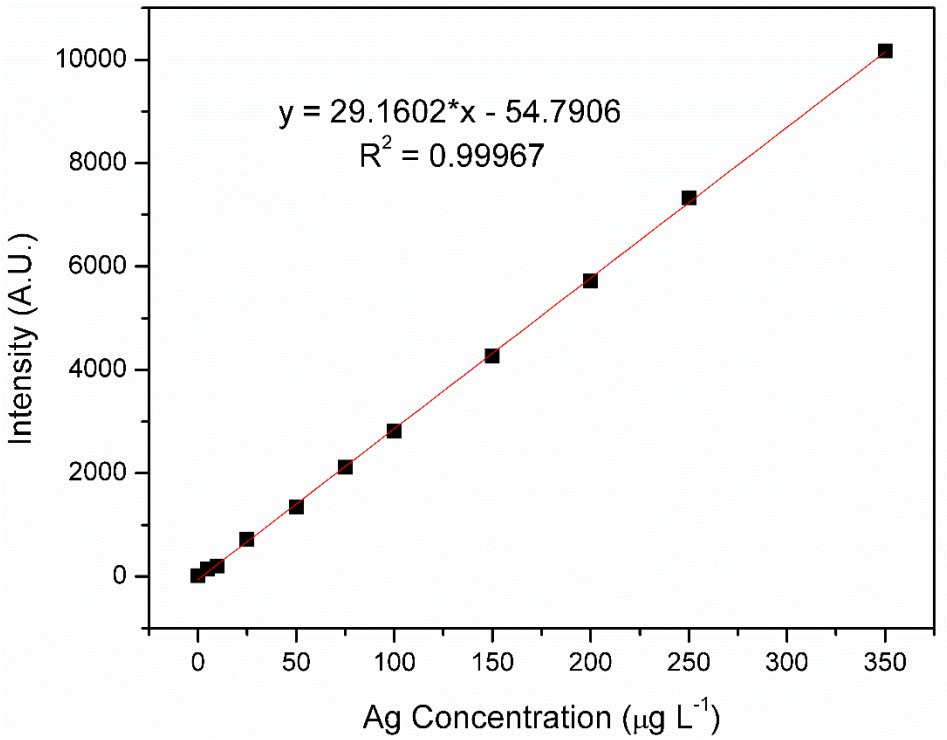

Figure 14. A representative ICP-OES 11-point external calibration curve together with the interpolation equation and R^2 value used to determine the total silver content in each sample.

Table 1 summarizes the ICP-OES results. It can be noted that AgNPs were lost in the supernatant during the centrifugation process. Approximately 325 mL of the original colloid of AgNPs was centrifuged, which resulted in ~ 80 mL of pellet containing AgNPs. The pellet was filtered through a 70 kD TFF filter, and ~ 5 mL of final colloid was attained.

Table 1. Total silver concentration of each colloid/supernatant throughout the centrifugation and TFF processes were determined via ICP-OES.

Sample	Ag Concentration (mg L^{-1})
Original colloid	104
0.2 µm filtrate	110
Supernatant of pellet	108
Supernatant of wash 1	9
70 kD permeate	6
70 kD retentate	156

To confirm the morphology and size-distribution of the starch-capped 70 kD retentate AgNPs, TEM was performed (Figure 15). It can be seen the starch-capped AgNPs are spherical in shape; as they can be visualized as darker black silver cores embedded in a lighter grey starch matrix. This was further confirmed by CytoViva images collected on the AgNP samples before (Figure 17A) and after (Figure 17B) purification through centrifugation and TFF.

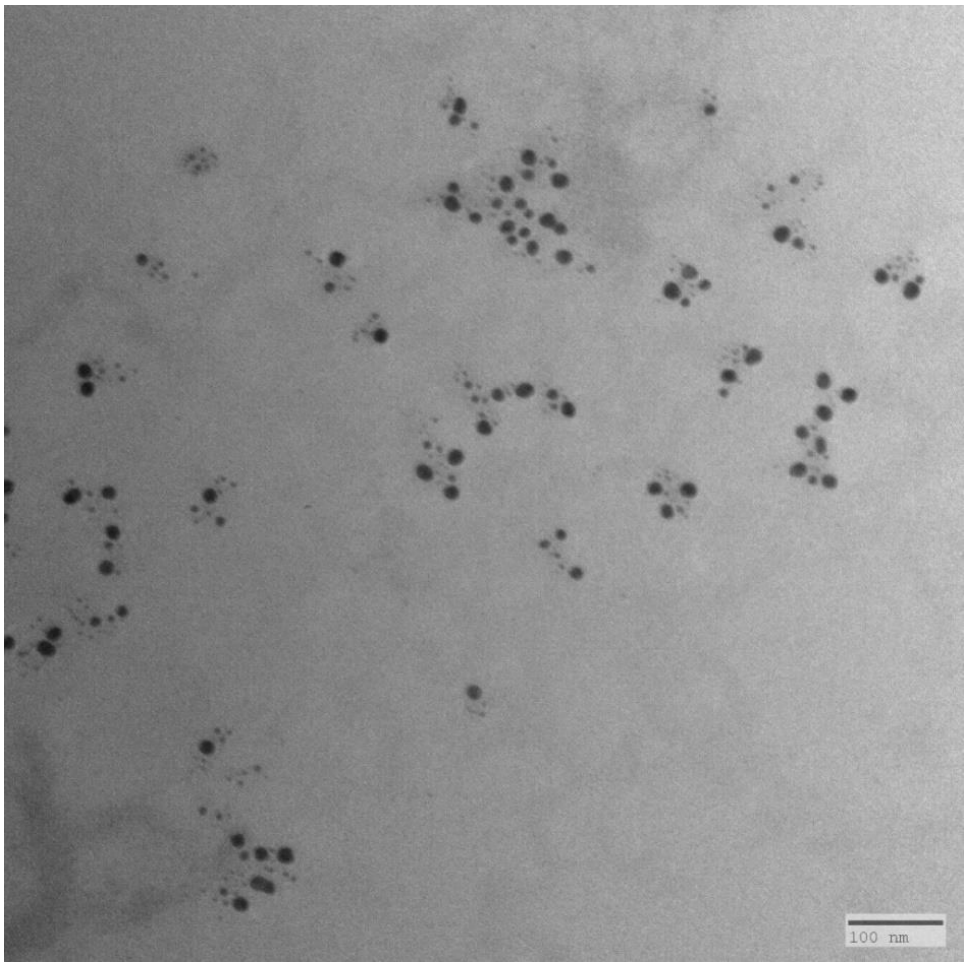

Figure 15. TEM micrograph of 70 kD retentate starch-capped AgNPs confirming morphology and size distribution.

Multiple TEM micrographs were utilized to create a histogram (N = 335) in ImageJ software (Figure 16). It was determined that the size distribution ranged from 4 nm to 24 nm with an average size of 9 ± 5.6 nm.

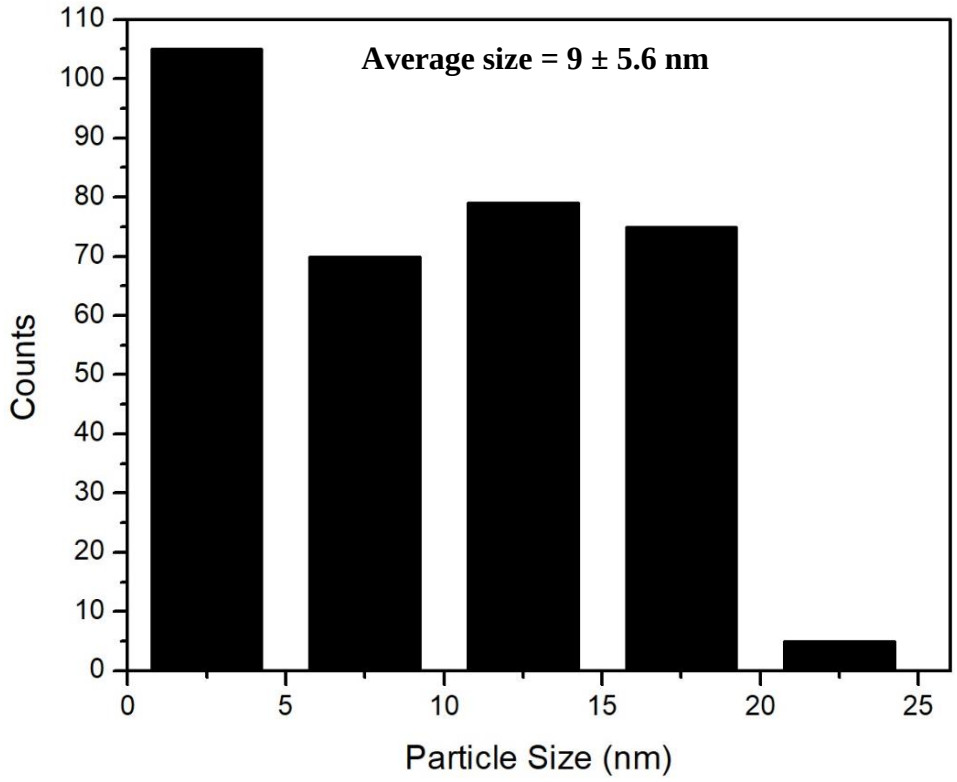

Figure 16. Histogram of particle size distribution (N = 335 AgNPs) compiled from TEM micrographs.

After confirming size and shape via TEM, CytoViva images and hyperspectral data were obtained on the 70 kD retentate starch-capped AgNPs (Figure 17). Spectra of the different colored AgNPs were collected (N = 30). This gives a spectral fingerprint and allows for the determination if the AgNPs are entering the cell and its organelles. Hyperspectral data were collected before and after the centrifugation/TFF processes to compare the spectral fingerprints.

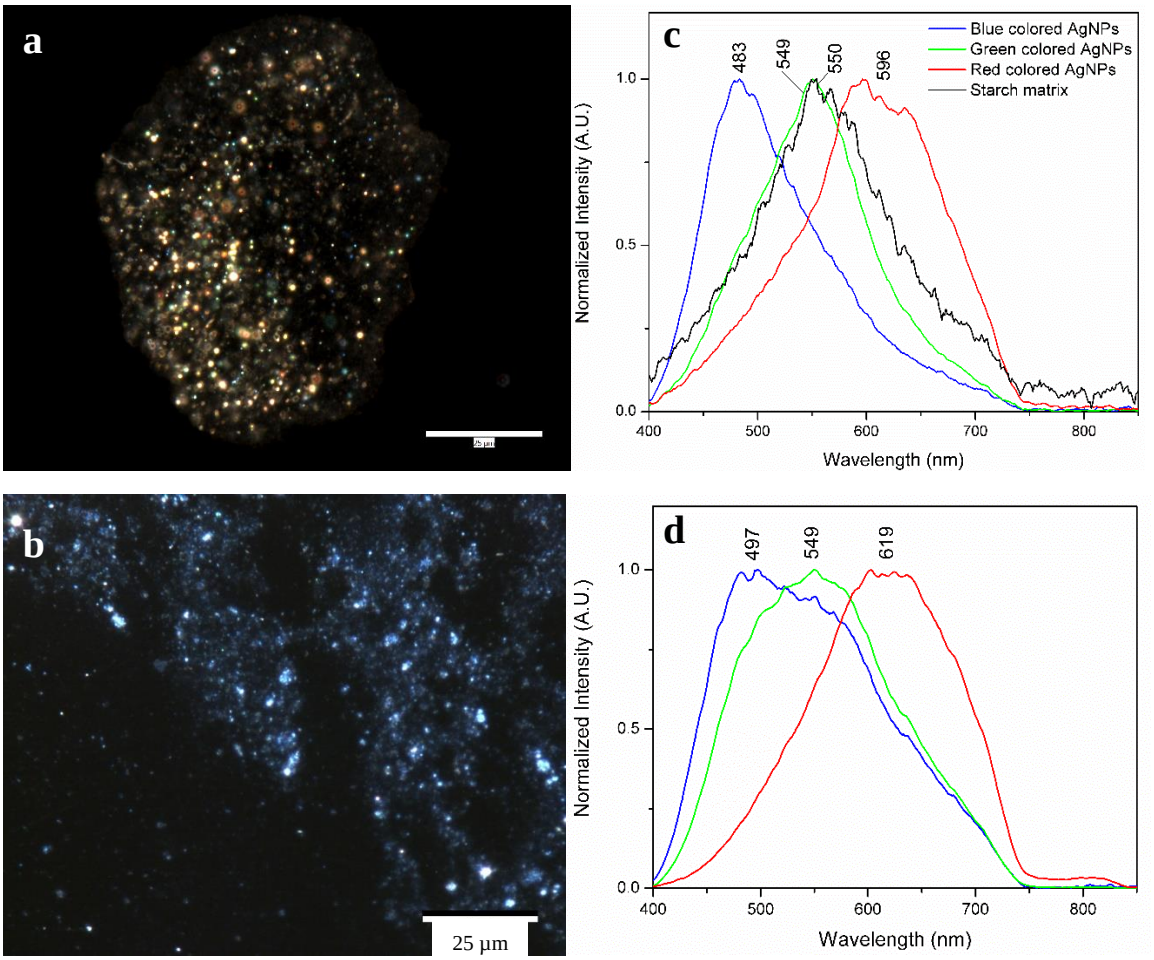

Figure 17. Characteristic CytoViva images of A) original starch-capped AgNP colloid, C) averaged hyperspectral of original starch-capped AgNP colloid, B) final 70 kD retentate starch-capped AgNPs and D) averaged hyperspectral of 70 kD starch-capped AgNPs used for cellular experiments (N = 30).

The full width half maximum values for the different colored AgNPs were calculated (Table 2).

Table 2. Surface plasmon resonance maxima and full width half maximum values of different colored AgNPs.

AgNP Sample	Maximum Wavelength (nm)	FWHM
Blue	497	187
Green	549	184
Red	619	170

3.2. Determination of Total Cellular Protein Content

The total cellular protein content determines the percentage of viable cells before and after exposure to AgNPs. A calibration curve was constructed from absorbance readings at 562 nm versus known concentrations of bovine albumin (Figure 18). This assay is employing the biuret reaction, which is the reduction of Cu^{+2} to Cu^{+1} by a protein in an alkaline medium and demonstrates a strong absorption at 562 nm.

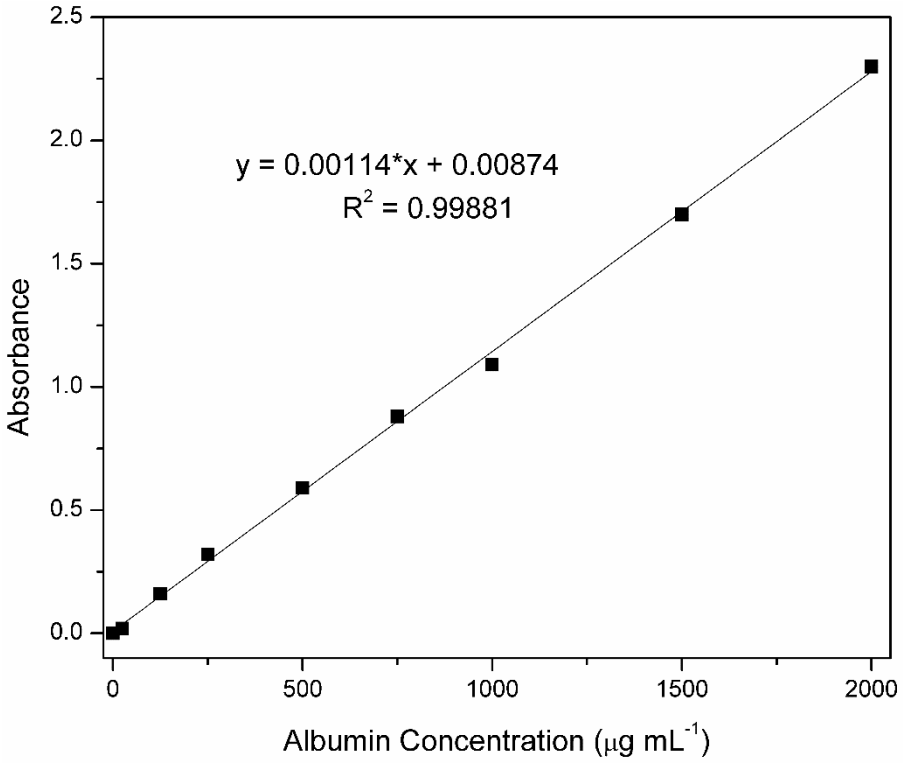

Figure 18. A representative absorbance 9-point external calibration curve together with the interpolation equation and R^2 value used to determine the total cellular protein content in each sample.

Utilizing the calibration curve made by serial dilutions from a 2 mg mL^{-1} bovine albumin standard, the total cellular protein content at each exposure concentration was determined by interpolation (Table 2).

Table 3. BCA assay data of total cellular protein content for each 4 hr exposure to AgNPs and vehicle control.

AgNP Exposure Concentration ($mg\ L^{-1}$)	Total Cellular Proteins ($\mu g\ mL^{-1}$)	Percentage of Viable Cells (%)
Vehicle Control	2600 ± 600	51
0.0	5100 ± 300	100
0.1	1100 ± 100*	21
1.0	1600 ± 200*	32
1.5	2300 ± 300*	46
3.0	400 ± 50	7

* No significant mean difference from each other (P = 0.2).

The total cellular protein content at 0.0 mg L^{-1} of AgNPs was 5100 µg mL^{-1}, which will be referred to as 100% viable cells. The vehicle control alone (2.2 mL of HQ H_2O in 47.8 mL of DMEM) reduced the number of viable cells by 49 % meaning that the amount of water added to the cells induced lysing. Despite the vehicle control having adverse effects on the cell population, a trend can still be seen with the addition of AgNPs. Exposure to 0.1, 1, 1.5, and 3 mg L^{-1} of AgNPs caused 79%, 68%, 54%, and 93% of viable cells to die, respectively. If the percent of the dead cells associated with the vehicle control (2.2 mL of HQ H_2O for each exposure) is subtracted from these percentages corresponding to AgNP exposures, 30%, 19%, 5%, and 43% of cell death was caused by 0.1, 1.0, 1.5, and 3.0 mg L^{-1}. More cell death occurred at lower concentrations, except at the highest concentration (3 mg L^{-1}). The effect of the vehicle control along with the AgNPs may be responsible for the higher cell deaths at exposure concentrations. At an exposure level of 3 mg L^{-1} of AgNPs, there was only 7% of viable cells. Thus, the mitochondrial isolation could not be performed at this exposure concentration. It would be expected that the percentage cell viability would decrease with increasing exposure concentrations. A one-way ANOVA was run to determine if there was any significant difference between the concentration exposures of 0.1, 1.0, and 1.5 mg L^{-1}. Based on a p-vale of 0.20, there is

not enough evidence to suggest there is a significant mean difference between any of the three concentrations. The trend seen in the data was not what was hypothesized, this might be because only three experiments were performed at each AgNP exposure concentration. Another reason for the trend in the data might be attributed to cellular growth. Even though the cell lines were all cultured under the same conditions, some may have differed in growth rate, leading to a different number of cells in each exposure plate.

3.3. Imaging of Exposed *Vero 76* Cells via CytoViva Hyperspectral Microscopy

Exposed *Vero 76* cells were imaged via CytoViva Hyperspectral Microscopy in order to observe the biodistribution of AgNPs within the cells. Cellular morphological changes were observed as a result of the AgNP exposure. All CytoViva samples were stained with MT-red to examine possible mitochondrial changes associated with the AgNP exposures.

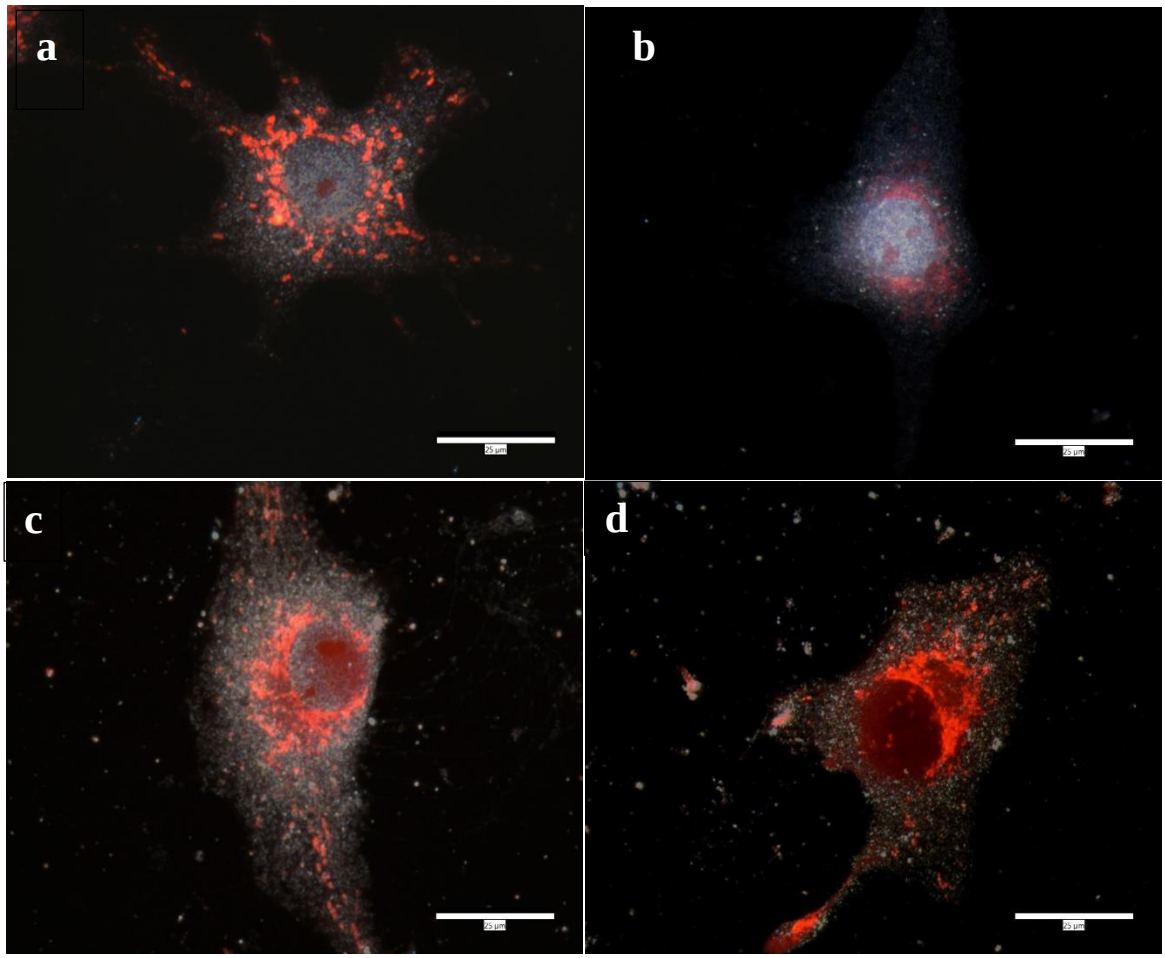

Figure 19. CytoViva optical images overlaid with fluorescence images of exposed *Vero 76* cells after exposure to a) 0, b) 0.1, c) 1.0, and d) 3.0 mg L^{-1} of starch-capped AgNPs for 2 hr. All cells were stained with 150 nM of Mito-tracker red dye prior to AgNP exposure. All scale bars are 25 µm.

Figure 19 displays the CytoViva optical images of cells superimposed on the corresponding fluoresence images after 2 hr exposure to various concentrations of AgNPs. In Figure 19a, the control image (0 mg L^{-1}) displays a healthy cell. It should be noted that these control cells exhibited normal the dendridic features and an even distribution of mitochondria throughout the cytoplasm. After exposure to 0.1 mg L^{-1} for 2 hr (Figure 19b), the mitochondria were no longer dispersed evenly within the cytoplasm.

As the exposure concentration increased, this trend increased as well. The morphology of the cell drastically changed with the increase of exposure concentration. In Figure 19c and Figure 19d, the cell shape is no longer smooth in appearance and looks compromised. These obsevations suggest that these cells might be in different stages of cell death. Figure 20 is comprised of the corresponding hyperspectral data for the above mentioned AgNP exposure concentrations at 2 hr. Data from all AgNPs seen on the cell were collected and then averaged in Origin.

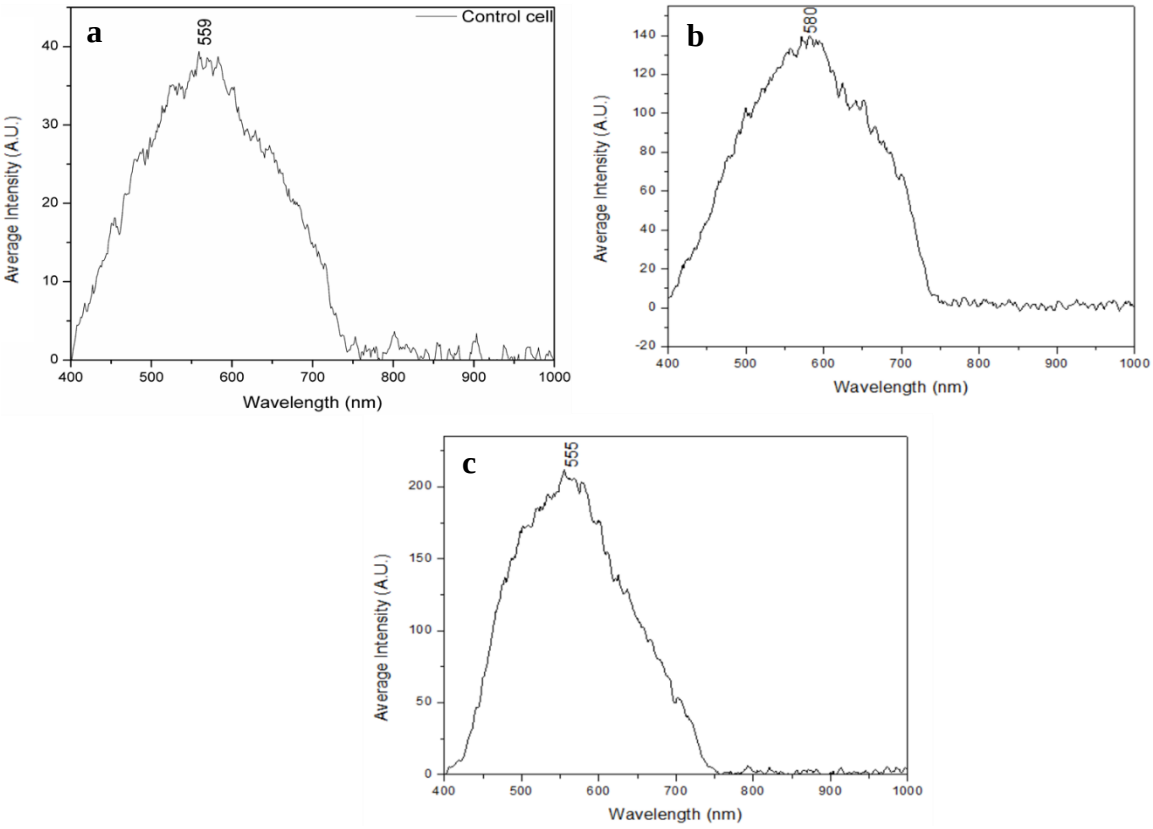

Figure 20. Corresponding hyperspectral data of *Vero 76* cells exposed to a) 0, b) 1.0, and c) 3.0 mg L^{-1} of AgNPs for 2 hr.

The control cell (0 mg L^{-1}) was observed to have a peak at 559 nm (Figure 20a). This spectral signature for the control remained constant at all exposure times. At 1 mg L^{-1}

exposures of AgNPs, it was observed that the spectral fingerprint widens ever so slightly (Table 4). This suggests that the AgNPs are interacting with the cell at the 1 mg L^{-1} AgNP exposure.

Table 4. Spectra maxima and full width half maximum of cell and AgNPs at each exposure concentration for 2 hr.

AgNPs Exposure Concentration (mg L^{-1})	Maximum Wavelength (nm)	FWHM
0	559	219
1	581	221
3	555	190

At 3 mg L^{-1} AgNP exposure, the peak obtained by averaging all AgNPs together, was narrower than the FWHM of the 0 mg L^{-1} control cell, but broader than any of the hyperspectral AgNPs. Thus, suggesting AgNPs are interacting with the cell.

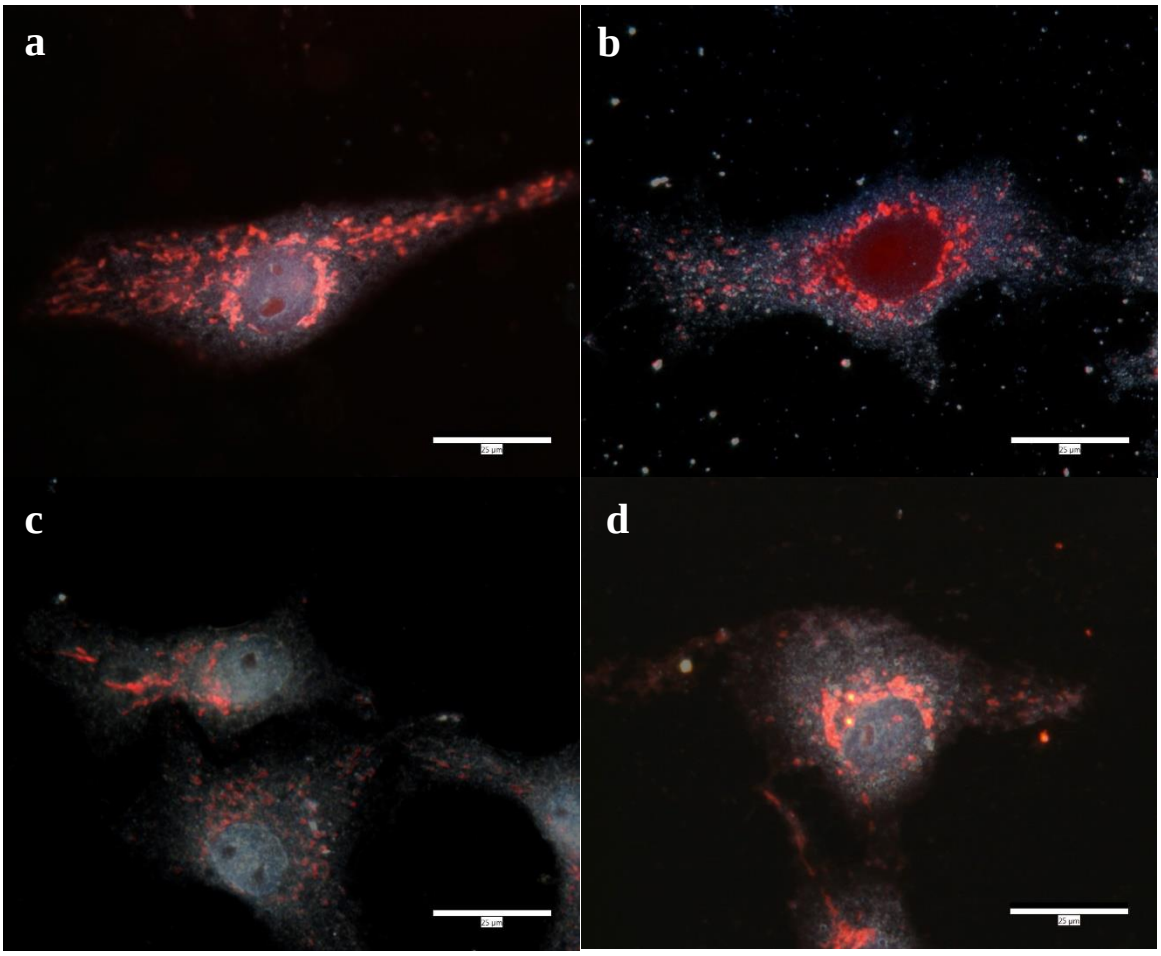

Figure 21. CytoViva optical images overlaid with fluorescence images of exposed *Vero 76* cells after exposure to a) 0, b) 0.1, c) 1.0, and d) 3.0 mg L^{-1} of starch-capped AgNPs for 4 hr. All cells were stained with 150 nM of Mito-tracker red dye prior to AgNP exposure. All scale bars are 25 µm.

Figure 21 displays the CytoViva optical images of cells superimposed on the corresponding fluorescence images after 4 hr exposure to various concentrations of AgNPs. Figure 21a displays the image of a healthy cell and even mitochondrial distribution. At an exposure concentration of 0.1 mg L^{-1} of AgNPs for 4 hr, the cell membrane appears rough, almost oval in shape, and cell debris was observed on the slide. As the exposure concentration was increased, the amount of cell debris on the slide increased and finding a fixed cell for imaging became more difficult. Figure 22 displays the corresponding averaged hyperspectral data for the various concentrations of AgNPs at the exposure time of 4 hr. Data from all AgNPs seen on the cell were collected and then averaged in Origin.

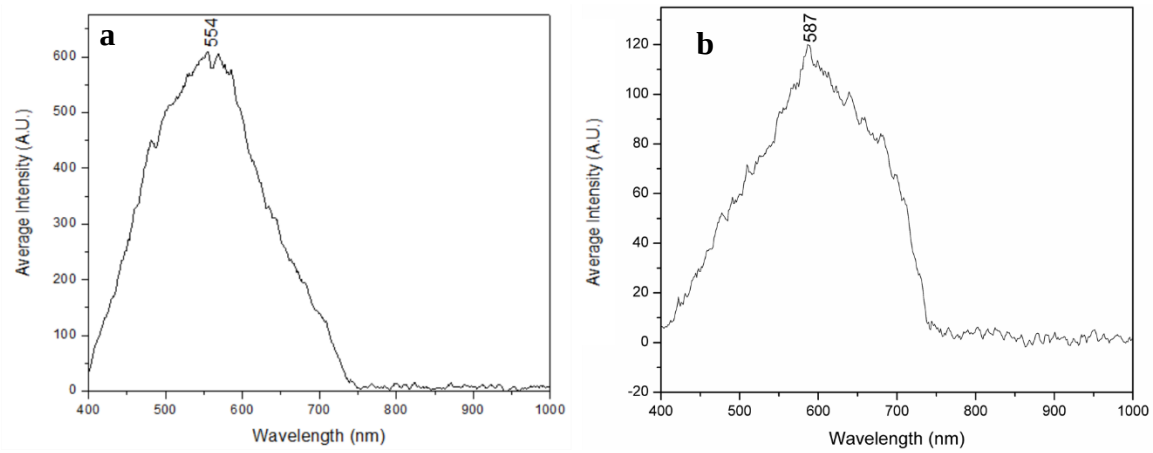

Figure 22. Corresponding hyperspectral data of *Vero 76* cells exposed to a) 1.0, and b) 3.0 mg L^{-1} of AgNPs for 4 hr.

Figure 22a and 22b, suggest interaction of AgNPs with the cells at exposure concentrations of 1.0 and 3.0 mg L^{-1}. This can be concluded based on the shifts in peak position and peaks FWHM (Table 5). The control cell peak corresponding to the 4 hr exposure to AgNPs was similar to the one after 2 hr exposure.

Table 5. Spectra maxima and full width half maximum of cell and AgNPs at each exposure concentration for 4 hr.

AgNPs Exposure Concentration (mg L^{-1})	Maximum Wavelength (nm)	FWHM
0	559	219
1	554	188
3	587	201

At the 1 mg L^{-1} AgNP exposure concentration, the FWHM was narrower than that of the 0 mg L^{-1} control cell, but wider than the FWHM of the AgNPs alone. This suggests there is interaction between the AgNP and the cell. The same observation was made at the 3 mg L^{-1} AgNP exposure concentration.

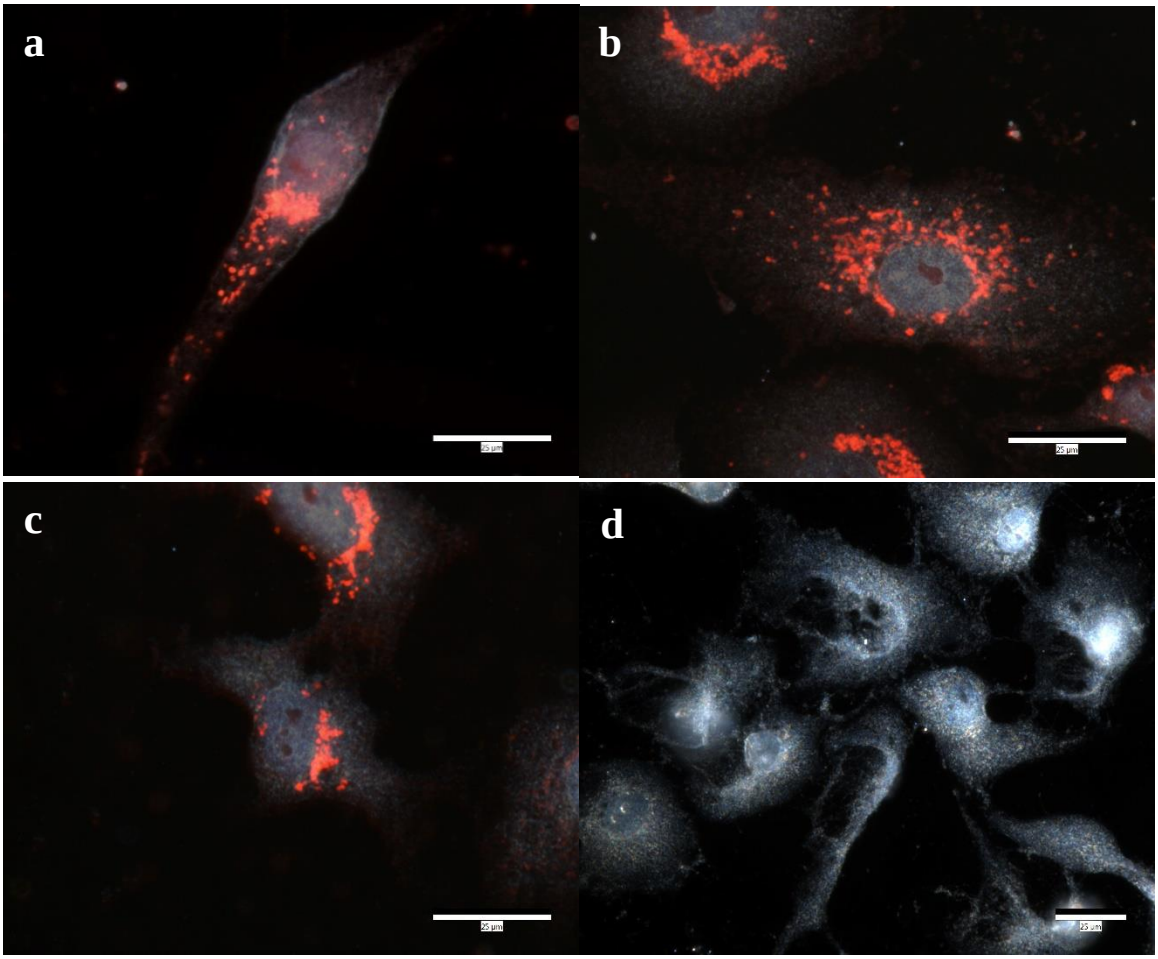

Figure 23. CytoViva optical images overlaid with fluorescence images of exposed *Vero 76* cells to a) 0, b) 0.1, c) 1.0, and d) 3.0 mg L^{-1} for 12 hr. All cells were stained with 100 nM Mito-tracker red dye prior to AgNP exposure. All scale bars are 25 µm.

Figure 23 displays the CytoVivia optical images of cells superimposed on the corresponding fluoresence images after 12 hr exposure at various concentrations of AgNPs. With increased exposure time, the toxicological effects of the AgNPs can clearly be observed. As the concentration was increased for this exposure time, the cell morphology was negatively impacted indicating cytotoxicity. At the highest exposure concentration of 3 mg L^{-1} of AgNPs, the cells were deformed. Furthermore, fluoresence images could not be collected to the the large amount of cell debris present on the slide at this concentration.

Figure 24 displays the corresponding hyperspectral data for the mentioned 12 hr exposures conditions.

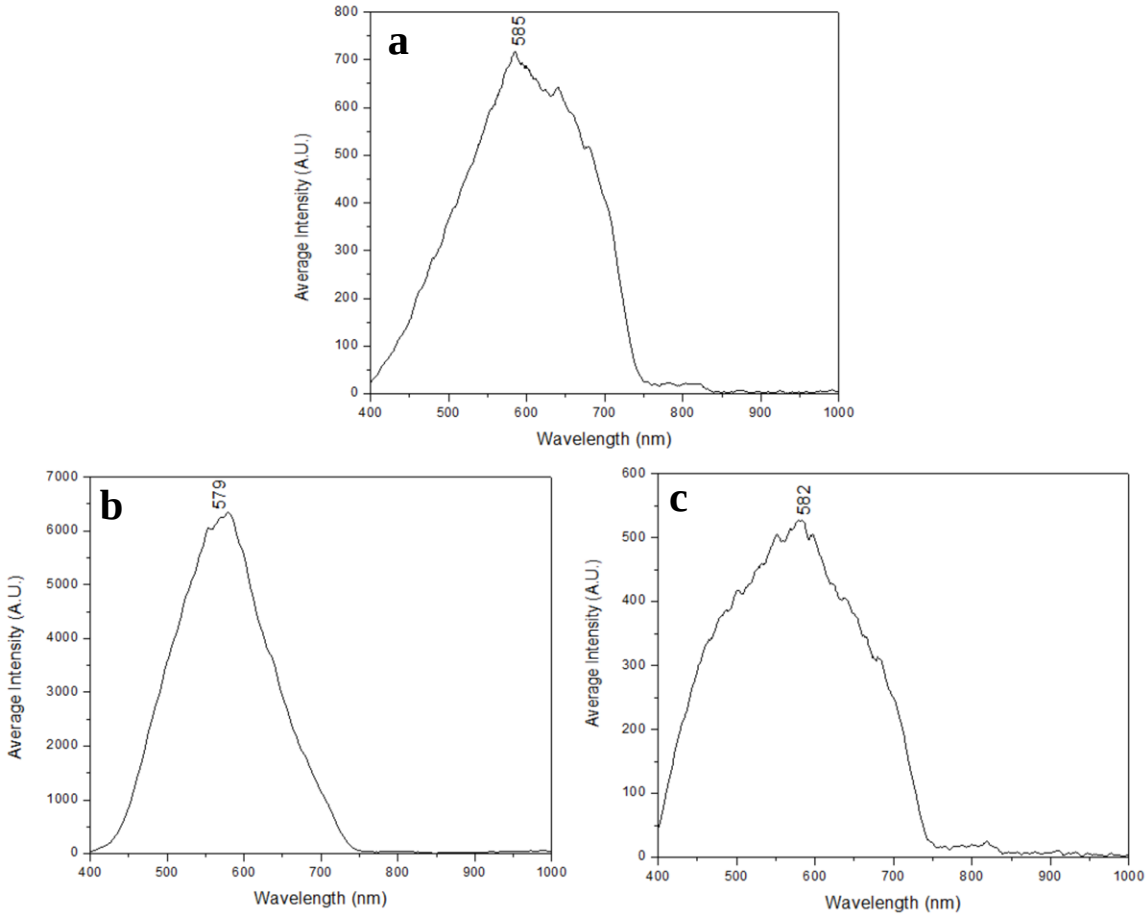

Figure 24. Corresponding hyperspectral data of Vero 76 cells exposed to at a) 0.1, b) 3.0, and c) 1.0 mg L^{-1} of AgNPs for 12 hr.

These hyperspectral data of all exposure concentrations of AgNPs suggest interaction of AgNPs with the cell. The strongest cellular interaction with AgNPs seemed to occur at the 1.0 mg L^{-1}; this had the broadest hyperspectral peak (Table 6).

Table 6. Spectra maxima and full width half maximum of cell and AgNPs at each exposure concentration for 12 hr.

AgNPs Exposure Concentration (mg L^{-1})	Maximum Wavelength (nm)	FWHM
0	559	219
0.1	585	210
1	582	252
3	579	152

From both the CytoViva images and hyperpectral data, it suggests that there is interaction between the AgNPs and the cell.

A two sample t-test was performed to determine if there was a significant difference between the FWHM at different exposure times and concentrations. When comparing the 2 hr and 4 hr exposure times, the p-value was determined to be 0.14 indicating no signicant difference. At the 2 hr and 12 hr exposure times, the p-value was determined to be 0.28, again indicating no significant difference. The p-value for the 4 hr and 12 hr exposure times was determined to be 0.47 showing no sigificant difference. Hyperspectral data and FWHM values for AgNP exposures at 1 and 3 mg L^{-1} were able to be collected for 2, 4, and 12 hr exposure times. A two sample t-test was performed to determine if there was any statistical significane between these FWHM values. The p-value was found to be 0.09, indicating no siginicant difference between these FWHM values at these exposure concentrations. Since the data is not signicantly different, a trend cannot be determined from the FWHM data. However, the CytoViva otpical image data suggests an interaction between the AgNPs and cell could be occuring.

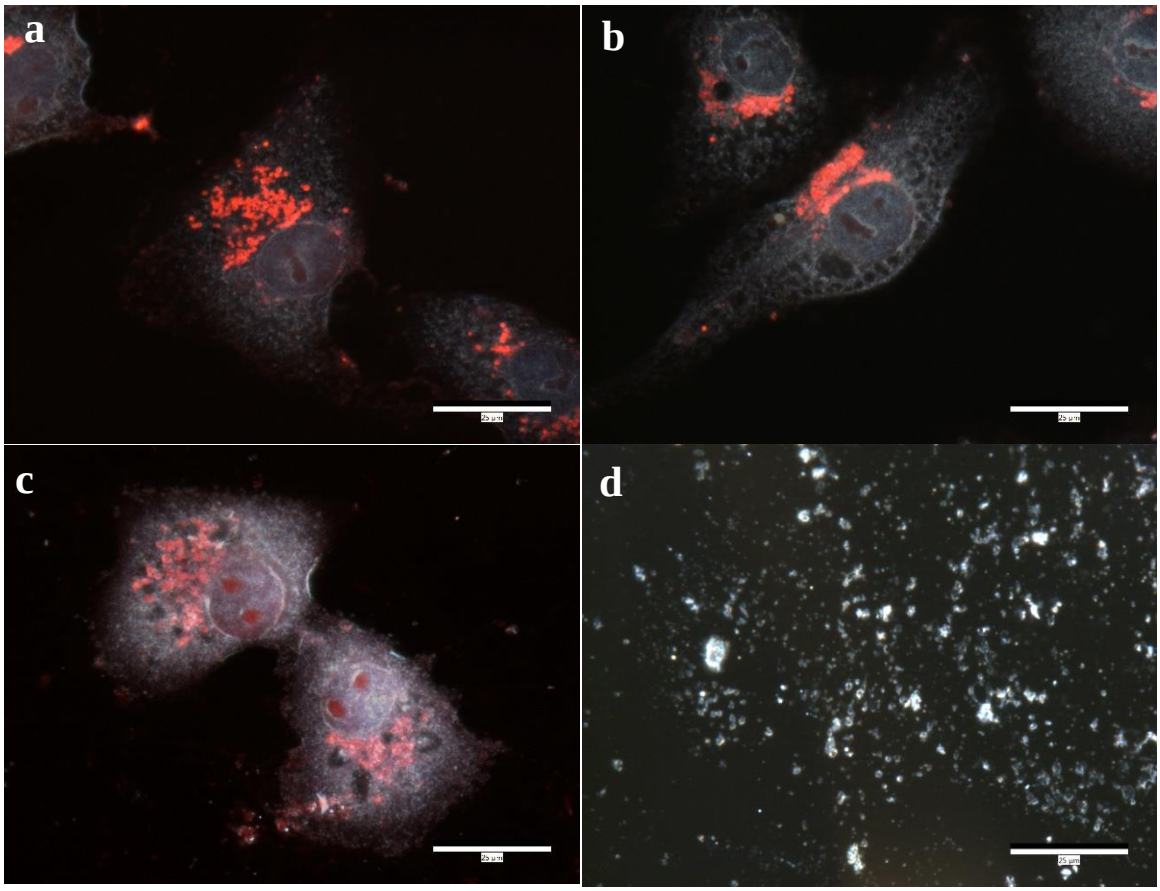

Figure 25. CytoViva optical images overlaid with fluorescence images of exposed *Vero 76* cells to a) 0, b) 0.1, c) 1.0, and d) 3.0 mg L^{-1} for 24 hr. All cells were stained with 100 nM Mito-tracker red dye prior to AgNP exposure. All scale bars are 25 µm.

Figure 25 displays the CytoViva optical images of cells superimposed on the corresponding fluorescence images after the 24 hr exposure to various concentrations of AgNPs. A similar trend was observed as in the 2, 4, and 12 hr exposures. The interaction of the AgNPs increased as the time and concentration were increased. This was confirmed by the hyperspectral data (Figure 26).

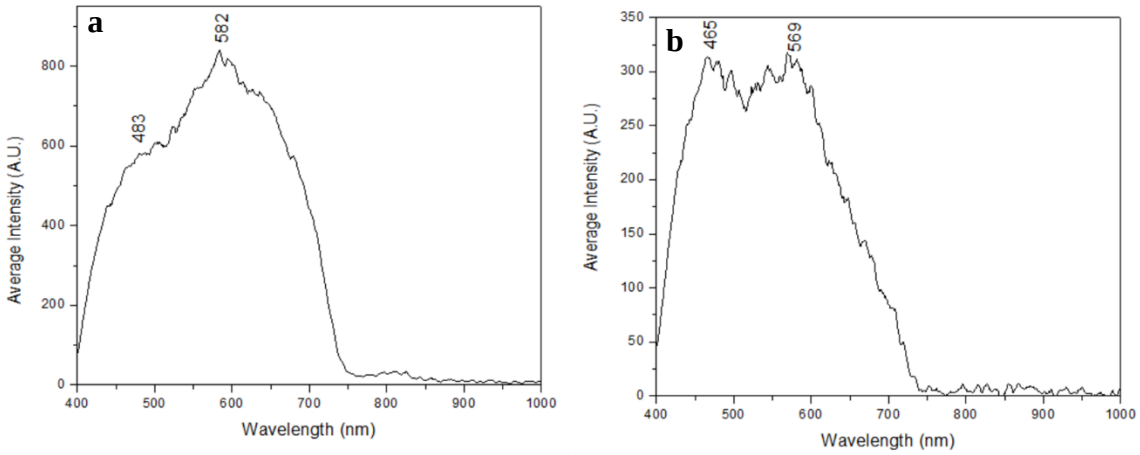

Figure 26. Corresponding hyperspectral data of Vero 76 cells exposed to a) 1.0, and b) 3.0 mg L^{-1} of AgNPs for 24 hr.

The hyperspectral data from both 1.0 and 3.0 mg L^{-1} were observed to have to 2 peaks. This may be occurring because of the AgNPs interaction with the cells are causing cell death and contents leaking out. FWHM could not be calculated for these exposures.

3.4. Analysis of Exposed *Vero 76* Cells by ICP-OES

During the mitochondrial isolation process, ten samples for each exposure (90 samples total) were collected and analyzed by ICP-OES. Eleven samples fell above the limit of detection (LOD), but only three samples were above the limit of quantification (LOQ) (Table 3). The LOD is 5.0 µg L^{-1} and LOQ is 3.0 µg L^{-1}.

Table 7. Silver concentration in exposed AgNP samples taken during the mitochondrial isolation process. Sample names are defined in Supporting Information Table S1.

Sample	AgNP Exposure Concentration (mg L^{-1})	Ag Concentration (µg L^{-1})	Percentage (%)
Incubated DMEM w/AgNPs	0.1	53*	53
Cytosol fraction	1	17*	2
Other cellular components	1	95*	10
PBS wash 1	1	72*	7
Incubated DMEM w/AgNPs	1	862	86
Mitochondria pellet	1.5	12*	1
Cytosol fraction	1.5	92*	6
Other cellular components	1.5	68*	5
DMEM supernatant 2	1.5	51*	3
PBS wash 1	1.5	151	10
Incubated DMEM w/AgNPs	1.5	1161	77

*Samples fell below the LOQ of 5 µg L^{-1}.

The samples above the LOQ show that most of the AgNPs remained in incubated DMEM w/AgNPs. At the 1 mg L^{-1} exposure, 86% of the AgNPs were found in the incubated DMEM. At 1.5 mg L^{-1}, 77% of the AgNPs remained in the incubated DMEM, while 10% of the AgNPs remained in the PBS wash 1. Samples above the LOD show that AgNPs are entering the cell, but the amount could not be report with accuracy. A repeated measures ANOVA was run to determine if there were any significant differences between the four AgNP exposure concentrations (0, 0.1, 1.0, and 1.5 mg L^{-1}) and at the various stages of the experiment ranging from sample 1 to sample 10. Since not all samples were above the LOD, not every sample is represented for each experiment. A level of significance of $\alpha = 0.05$ was used to assess statistical significance and SAS version 9.4 was used for all analyses. Statistical analysis was run by the Statistics Consulting Center at Wright State University. Descriptive statistics for ICP-OES analysis are in Table 8.

Table 8. Descriptive statistics for ICP-OES analysis by concentration and sample. Sample names defined in Supporting Information Table S1.

AgNP Exposure Concentration (mg L^{-1})	Sample	N	Mean	Std Dev	Minimum	Maximum
0	PBS wash 1	6	63.83	27.87	29.33	108.12
	Media supernatant	3	63.88	28.51	36.44	93.36
	Other cellular components	9	129.2	28.07	65.95	164.79
	Cytosol fraction	3	70.03	7.59	63.61	78.4
	Mitochondria pellet	3	67.88	17.79	49.9	85.48
0.1	Incubated DMEM w/AgNPs	9	151.65	14.99	130.25	176.46
1	Incubated DMEM w/AgNPs	9	1124.45	206.23	875.35	1395.41
	PBS wash 1	9	173.88	38.85	109.16	244.59
	Other cellular components	9	202.33	61.39	139.54	279.78
	Cytosol fraction	6	110.37	26.03	79.24	148.49
1.5	Incubated DMEM w/AgNPs	9	1483.8	92.07	1353.51	1600.99
	PBS wash 1	9	269.76	47.08	211.56	343.95
	Media Supernatant	9	148.72	32.25	108.14	207.41
	Other cellular components	9	169.62	25.63	116.57	199.09
	Cytosol fraction	9	198.11	42.23	129.27	250.48
	Mitochondria pellet	9	102.11	22.79	70.57	131.59

From the descriptive statistics in Table 8, 45 comparisons of interest were made. Of those 45 comparisons, 31 compared the ICP-OES mean values between samples within the same concentration, and 14 compared the ICP-OES mean values of the samples within the same concentration. A stepdown Bonferroni multiple comparison procedure was utilized in order to control the potential for type I error rate, this is when significance is claimed, but there are none. A confidence level of 95 % at most was utilized, this was calculated via Bonferroni multiple comparison procedure. These results are contained in Supporting Information (Table S2).

Samples within the AgNP exposure concentration 0 mg L^{-1}, there was not adequate evidence to suggest any significant differences among all comparisons (all p-values were 0.99). At AgNP exposure concentration 0.1 mg L^{-1}, there was only one sample that was above the LOD, therefore no comparisons between samples at this concentration could be made.

Samples within AgNP exposure concentration 1.0 mg L^{-1}, there is strong evidence suggesting a significant mean difference between sample 1 and sample 2 (p-vale < 0.0001). A significant mean difference between sample 1 and sample 7, having a p-value of < 0.001. There was also strong evidence suggesting there is a mean difference between sample 1 and sample 8 (p-value < 0.0001). No other significant differences were detected.

Samples within the AgNP exposure concentration 1.5 mg L^{-1}, there was strong evidence suggesting a significant mean difference between: sample 1 and sample 2, sample 1 and sample 6, sample 1 and sample 7, sample 1 and sample 8, sample 1 and sample 10. All comparisons with a significant mean difference had a p-value of < 0.0001. No other significant differences were detected within the samples at this concentration.

The only comparison that could be made between different AgNP exposure concentrations were with sample 1. There was strong evidence suggesting a significant mean difference between sample 1 for the following concentrations: 0.1 and 1.0 mg L^{-1}, 0.1 and 1.5 mg L^{-1}, 1 and 1.5 mg L^{-1}. Between AgNP exposure concentrations 0.1 and 1.0 mg L^{-1}, the p-value was determined to be < 0.0001. The p-value between AgNP exposure concentrations 0.1 and 1.5 mg L^{-1} was also < 0.0001. Lastly, between AgNP exposure

concentrations 1.0 and 1.5 mg L^{-1}, the p-value was determined to equal 0.0005. No other significant differences were detected.

All significant differences detected involved sample 1, however, data for sample 1 at 0 mg L^{-1} was not reliable, therefore no conclusions could be drawn about it relative to other samples at 0 mg L^{-1} or compared to other concentrations at sample 1. No conclusions could be drawn at the AgNP exposure concentration 0.1 mg L^{-1} due to only sample 1 data being above the LOD.

4. Conclusions

From CytoViva images, it was observed as concentration of AgNPs and time increased, more cell death occurred, which correlates to the proposed hypothesis. This could be clearly seen by the morphological changes to cell shape as the time and concentration of AgNPs was increased. From the hyperspectral data collected of exposed cells at various concentrations, it suggests that there is interaction between the cell and AgNPs. In the future, implementing the 3-D camera on CytoViva would help determine if the AgNPs are interacting with the cell wall and/or have entered the cytosol. This would give insight into the possible mechanism of how AgNPs are entering the cell and causing cell death.

From ICP-OES data, it was determined that there were significant mean differences between some samples within the same concentration and between sample 1 at different exposure concentrations. It can be concluded that AgNPs did enter the mitochondria of the cells, however, the amount could not be quantified. To produce more accurate results, concentrations used for exposures need to be increased and the exposure time should be increased as well to increase the chances of AgNPs entering the mitochondria. The sample preparation of biological samples for ICP-OES should also be adjusted to a smaller dilution factor.

The AgNP synthesis could be optimized for a higher yield. Perhaps less starch could be used, eliminating the purification via centrifugated step. Also, doing a large batch-wise process, larger surface area TFF filter, and a peristaltic pump would increase yield and efficiency. It was observed that the colloid became gel-like when the excess starch was

not removed before filtration of the original colloid. A future application of starched-capped AgNP synthesis, could be to use this gel-like colloid in the medical field, perhaps in a burn gel.

The main aim of this study was to determine if AgNPs were entering the mitochondria of *Vero 76* cells, quantify the total silver content, and look at AgNP distribution within the cell. It was determined AgNPs are entering the cell, but the ICP-OES signal fell below the LOQ. To quantify the total silver content within these biological matrices, the exposure concentrations of AgNPs should be increased and the dilution factor used in sample preparation decreased.

Future Raman spectroscopy experiments should be performed to investigate the mechanism of AgNP formation and of AgNP-cellular interaction. CytoViva 3-D imaging should be employed to give insight if the AgNP is interacting with the cellular wall and/or components inside the cell. Lastly, MTT and ROS assays should also be performed to investigate cellular metabolic activity and the cause of cell death.

5. References

1. The Nanodatabase. DTU Environment, Danish Ecological Council and Danish Consumer Council: 2019.(Accessed November 2019)
2. EPA, Technical Fact Sheet - Nanomaterials. Agency, E. P., Ed. 2017.
3. Fabrega, J.; Fawcett, S. R.; Renshaw, J. C.; Lead, J. R., Silver Nanoparticle Impact on Bacterial Growth: Effect of pH, Concentration, and Organic Matter. *Environmental Science & Technology* **2009,** *43* (19), 7285-7290.
4. National Science Foundation - Where Discoveries Begin. https://www.nsf.gov/news/news_summ.jsp?cntn_id=130586 (accessed October 2018).
5. Consumer Products Inventory. http://www.nanotechproject.org/cpi/products/ (accessed September 2018).
6. Petica, A.; Gavriliu, S.; Lungu, M.; Buruntea, N.; Panzaru, C., Colloidal silver solutions with antimicrobial properties. *Materials Science & Engineering B* **2008,** *152* (1), 22-27.
7. Hajipour, M. J.; Fromm, K. M.; Akbar Ashkarran, A.; Jimenez de Aberasturi, D.; Larramendi, I. R. d.; Rojo, T.; Serpooshan, V.; Parak, W. J.; Mahmoudi, M., Antibacterial properties of nanoparticles. *Trends in Biotechnology* **2012,** *30* (10), 499-511.
8. Markopoulos, M. M., *Antimicrobial Activity of Fractionated Borohydride-Capped and Electrochemical Colloidal Silver*. Wright State University / OhioLINK: 2017.
9. Thomas, R.; Janardhanan, A.; Varghese, R. T.; Soniya, E. V.; Mathew, J.; Radhakrishnan, E. K., Antibacterial properties of silver nanoparticles synthesized by marine Ochrobactrum sp. *Brazilian Journal of Microbiology* **2014,** (4), 1221.
10. Asharani, P. V.; Lian Wu, Y.; Gong, Z.; Valiyaveettil, S., Toxicity of silver nanoparticles in zebrafish models. *Nanotechnology* **2008,** *19* (25), 255102-255102.
11. AshaRani, P. V.; Low Kah Mun, G.; Hande, M. P.; Valiyaveettil, S., Cytotoxicity and genotoxicity of silver nanoparticles in human cells. *ACS Nano* **2009,** *3* (2), 279-290.
12. Han, J.; Gurunathan, S.; Jeong, J.-K.; Choi, Y.-J.; Kwon, D.-N.; Park, J.-K.; Kim, J.-H., Oxidative stress mediated cytotoxicity of biologically synthesized silver nanoparticles in human lung epithelial adenocarcinoma cell line. *Nanoscale Research Letters* **2014,** *9* (1), 1-14.
13. Kim, Y. S.; Kim, J. S.; Cho, H. S.; Rha, D. S.; Kim, J. M.; Park, J. D.; Choi, B. S.; Lim, R.; Chang, H. K.; Chung, Y. H.; Kwon, I. H.; Jeong, J.; Han, B. S.; Yu, I. J., Twenty-Eight-Day Oral Toxicity, Genotoxicity, and Gender-Related Tissue Distribution of Silver Nanoparticles in Sprague-Dawley Rats. *Inhalation Toxicology* **2008,** *20* (6), 575-583.
14. Lima, R.; Seabra, A. B.; Durán, N., Silver nanoparticles: a brief review of cytotoxicity and genotoxicity of chemically and biogenically synthesized nanoparticles. *Journal of Applied Toxicology* **2012,** *32* (11), 867-879.

15. EPA Drinking Water Regulations and Contaminants. https://www.epa.gov/dwregdev/drinking-water-regulations-and-contaminants (accessed May 2018).
16. Rosa, A. H. L.; Yan, M.; Fernández, R. F.; Wang, X.; Zegarra, E., Top-down and Bottom-up approaches to nanotechnology An overview in the context of developing Proton-fountain Electric-field-assisted Nanolithography (PEN) : Fabrication of polymer nanostructures that respond to chemical and electrical stimuli *Material Science* **2013**.

17. Mohan, S.; Oluwafemi, O. S.; Songca, S. P.; Jayachandran, V. P.; Rouxel, D.; Joubert, O.; Kalarikkal, N.; Thomas, S., Synthesis, antibacterial, cytotoxicity and sensing properties of starch-capped silver nanoparticles. *Journal of Molecular Liquids* **2016,** *213*, 75-81.
18. Ortega-Arroyo, L.; Martin-Martinez, E. S.; Aguilar-Mendez, M. A.; Cruz-Orea, A.; Hernandez-Pérez, I.; Glorieux, C., Green synthesis method of silver nanoparticles using starch as capping agent applied the methodology of surface response. *Starch - Stärke* **2013,** *65* (9-10), 814-821.
19. Vigneshwaran, N.; Nachane, R. P.; Balasubramanya, R. H.; Varadarajan, P. V., A novel one-pot 'green' synthesis of stable silver nanoparticles using soluble starch. *Carbohydrate Research* **2006,** *341* (12), 2012-2018.
20. Machalek, A. Z., How Cells Eat In. *LiveScience* 2013.
21. Mesa, K., Essential Cell Biology. *Yale J Biol Med* **2015,** *88* (1), 100-101.
22. Ammerman, N. C.; Beier-Sexton, M.; Azad, A. F., Growth and maintenance of Vero cell lines. *Current Protocols In Microbiology* **2008,** *Appendix 4*, 4E-4E.
23. Dorney, K. M.; Baker, J. D.; Edwards, M. L.; Kanel, S. R.; O'Malley, M.; Pavel Sizemore, I. E., Tangential Flow Filtration of Colloidal Silver Nanoparticles: A "Green" Laboratory Experiment for Chemistry and Engineering Students. *Journal of Chemical Education* **2014,** *91* (7), 1044-1049.
24. Carey, D. M.; Korenowski, G. M., Measurement of the Raman spectrum of liquid water. *The Journal of Chemical Physics* **1998,** *108* (7), 2669-267

6. Supporting Information

Table S1. List of sample names for each step of the mitochondrial isolation assay.

Sample Number	Sample Name
1	Incubated DMEM w/AgNPs
2	PBS wash 1
3	PBS wash 2
4	PBS wash 3
5	Media supernatant 1
6	Media supernatant 2
7	Other Cellular components
8	Cytosol fraction
9	Mitochondrial pellet wash
10	Mitochondria pellet

Table S2. Statistical summary of the stepdown Bonferroni procedure for ICP-OES measurements utilizing a 95% confidence level.

Comparison (mg L^{-1})	Estimate	Standard Error	p - value
Concentration 0: Sample 2 - 6	-0.05	99.38	0.99
Concentration 0: Sample 2 - 7	-65.37	74.07	0.99
Concentration 0: Sample 2 - 8	-6.2	99.38	0.99
Concentration 0: Sample 2 - 10	-4.05	99.38	0.99
Concentration 0: Sample 6 - 7	-65.32	93.7	0.99
Concentration 0: Sample 6 - 8	-6.15	114.75	0.99
Concentration 0: Sample 6 - 10	-4	114.75	0.99
Concentration 0: Sample 7 - 8	59.17	93.7	0.99
Concentration 0: Sample 7 - 10	61.32	93.7	0.99
Concentration 0: Sample 8 - 10	2.15	114.75	0.99
Concentration 1: Sample 1 - 2	950.58	66.25	< 0.0001
Concentration 1: Sample 1 - 7	922.12	66.25	< 0.0001
Concentration 1: Sample 1 - 8	1014.08	74.07	< 0.0001
Concentration 1: Sample 2 - 7	-28.45	66.25	0.99
Concentration 1: Sample 2 - 8	63.51	74.07	0.99
Concentration 1: Sample 7 - 8	91.96	74.07	0.99

Concentration 1.5: Sample 1 - 2	1214.04	66.25	< 0.0001
Concentration 1.5: Sample 1 - 6	1335.08	66.25	< 0.0001
Concentration 1.5: Sample 1 - 7	1314.18	66.25	< 0.0001
Concentration 1.5: Sample 1 - 8	1285.7	66.25	< 0.0001
Concentration 1.5: Sample 1 - 10	1381.7	66.25	< 0.0001
Concentration 1.5: Sample 2 - 6	121.04	66.25	0.99
Concentration 1.5: Sample 2 - 7	100.14	66.25	0.99
Concentration 1.5: Sample 2 - 8	71.66	66.25	0.99
Concentration 1.5: Sample 2 - 10	167.65	66.25	0.62
Concentration 1.5: Sample 6 - 7	-20.9	66.25	0.99
Concentration 1.5: Sample 6 - 8	-49.38	66.25	0.99
Concentration 1.5: Sample 6 - 10	46.61	66.25	0.99
Concentration 1.5: Sample 7 - 10	-28.48	66.25	0.99
Concentration 1.5: Sample 7 - 8	67.52	66.25	0.99
Concentration 1.5: Sample 8 - 10	96	66.25	0.99
Sample 1: 0.1 - 1	-972.8	66.25	< 0.0001
Sample 1: 0.1 - 1.5	-1332.15	66.25	< 0.0001
Sample 1: 1 - 1.5	-359.35	66.25	0.0005
Sample 2: 0 - 1	-110	93.7	0.99
Sample 2: 0 - 1.5	-205.88	93.7	0.99
Sample 2: 1 - 1.5	-95.89	66.25	0.99
Sample 6: 0 - 1.5	-19.52	66.25	0.99
Sample 7: 0 - 1	-132.3	93.7	0.99
Sample 7: 0 - 1.5	-99.59	93.7	0.99
Sample 7: 1 - 1.5	32.71	66.25	0.9
Sample 8: 0 - 1	-40.34	99.38	0.99
Sample 8: 0 - 1.5	-128.07	93.7	0.99
Sample 8: 1 - 1.5	-87.74	74.07	0.99
Sample 10: 0 - 1.5	-34.23	93.7	0.99